© NOV 2025 | IRE Journals | Volume 9 Issue 5 | ISSN: 2456-8880
DOI: https://doi.org/10.64388/IREV9I5-1712089

Protective Efficiency of Bio-Inhibitors and Adsorption Isotherms: A Review

NWACHUKWU SAMUEL UGOCHUKWU[1], DR. E.O. OBIDIEGWU (ASSOC. PROF.)[2], PROF S.O. ADEOSUN[3]

[1, 2, 3]*Department of Metallurgical and Materials Engineering, University of Lagos*

Abstract- ***Corrosion inhibitors made of various non-chromates have been employed in place of ecologically dangerous chromates, and plant extracts are at the top of the list. Currently, a large number of compounds that are sold commercially harm human safety, whether used in the field, handled, or synthesised as inhibitors. Green corrosion inhibitors are compounds that are ecologically biocompatible, biodegradable, and nontoxic. Typically, they are composed of trash or extracts from natural plants, both of which are widely accessible in many nations. To prevent (initiation and/or propagation) the corrosion process, the majority of green inhibitor molecules used often consist of multiple bonds, aromatic rings, polar functional groups, and electronegative atoms such as P, N, S, or O that can work in coordination with metal cations to form protective layers(films) on the reinforcements' metallic surfaces. Numerous surface examination methods, including AFM, FTIR, UV, fluorescence spectra, and SEM, have been used to examine inhibitive films.***

Keywords: ***Green Corrosion Inhibitor, Films, Plants, Non-Toxic, Extract.***

I. INTRODUCTION

Concerns regarding the toxicity of corrosion inhibitors in business are growing. The planet is gradually becoming poisoned by harmful compounds, in addition to harming living things. Corrosion inhibitors are a crucial piece of techniques for reducing corrosion, much like coatings. Inhibitors have several applications in the field of corrosion engineering in the fight against corrosion, with several studies carried out in this area of engineering.

Corrosion is a natural chemical process that converts metals into their more chemically stable state, like hydroxide, sulphide, and oxide. It is a major problem with engineering products and occurs in facilities such as pipelines conveying gas produced from drilling, gathering, storage, and distribution stages. The production of environmentally friendly and economical corrosion inhibitors is necessary for the practical application of this idea. Inhibitors have been in existence and in use for many years to lessen severe corrosion issues brought on by corrosion agents like CO_2, H_2S, etc. Green inhibitors, mostly plant extracts, have substituted the conventional metal corrosion inhibitors in recent years.

Corrosion inhibitors are one of the several methods used to retardate or slow down corrosion in gas pipelines. Other methods used in the fight against corrosion include cathodic protection (Anees & Khalid, 2012), organic coatings, and the application of first-class corrosion-resistant alloys, which can be put to use in the fight against corrosion, forming inhibitor films which are still known to be an unequalled technique of defence against corrosion in acidic environments. The inhibitors forming films are often used in industries to create a molecular layer on the surface of the steel and aliphatic tail as an additional layer in hydrocarbon to stop water from making contact with the steel surface (Kausalya & Hazlina, 2020).

Preparing an extract usually entails gathering the plant materials, cleaning and washing them, drying and crushing them, pasting and powdering them, dissolving them, stirring and extracting them in a particular solvent or solvents, and storing them. As a medium for extracts, both organic and aqueous solvents are employed. Polar phytochemicals are often found in aqueous extracts, while non-polar phytochemicals are found in organic extracts. The main types of phytochemicals that suppress corrosion include tannins, phlobatannins, antraquinones, amino acids, glycosides, alkaloids, flavonoids, phytosterols, saponins, steroids, and phenolic compounds, among others. Polar functional groups, such as hydroxyl (–OH), amino (−NH_2), amide (–$CONH_2$), acid chloride (–COCl), carboxylic acid (–COOH), ester (–$COOC_2H_5$), etc., are present in these phytochemicals and aid in their adsorption (Alrefaee, Rhee, Verma, Quraishi, & Ebenso, 2021)

1.1 Background

Green inhibitors are inhibitors that are nontoxic to the environment in which they are used; they are plant extracts, and they are high in demand when compared to commercial inhibitors (Hussin, Rahim, Mohamad Ibrahim, & Brosse, 2015; Negm, Kandile, Aiad, & Mohammad, 2011). These are plant extracts that are green and sustainable, with natural and biological properties and are capable of inhibiting metals and alloys from corroding (Chemat, Vian, & Cravotto, 2012). The leaf is the most preferred section of the plant because of its number of synthesised phytochemicals, or active components, which function similarly to pharmaceutical inhibitors. It is essential to recognise that the extract of other plant components, including roots, bark, flowers, fruits, wood, seeds, and peels, have all contributed to the efficacy of inhibition (El-Etre, 2008; Ji, Dwivedi, Sundaram, & Prakash, 2016). Furthermore, carbon dioxide, a very harmful greenhouse gas, is necessary for the photosynthetic process in phytochemical synthesis, which lends credence to the concept of "green chemistry (Kausalya, & Hazlina, 2020).

When applied at extremely low concentrations, the green corrosion inhibitors prevent the metal surface from coming into contact with a corrosive substance. Plant extracts influence the anodic or cathodic reaction kinetics, which in turn affects the rate of dilation of hostile ions from interacting with the metal surface, hence affecting the pace of corrosion via the adsorption process on the metal surface thus, by raising the metal surface's electrical resistance, a film layer can be created (Krishnaveni, & Ravichandran, 2014). Furthermore, it is commonly recognised that green corrosion inhibitors include adsorptive qualities, or site-blocking components, which allow the plant extract's active molecules to be adsorbed on the exposed metal surfaces (Sanatkumar, Nayak, & Nityananda Shetty, 2012). Equation 1.1 illustrates how the inhibitor molecules function by adsorption on the metal surface as neutral molecules rather than hydrogen ions (Manamela, Murulana, Kabanda, & Ebenso, 2014).

$$\text{Inhibitor} + n\text{H}_{ads} \rightarrow \text{Inhibitor}_{ads} + \text{H}_2 \qquad 1.1$$

where ${}_n\text{H}_{ads}$ is adsorbed hydrogen ions sourced from water, and Inhibitor_{ads} are adsorbed neutral molecules sourced from plant extract.

Alongside this, there are a few restrictions that need to be considered while making plant extracts. Typically, the extraction solvents will diffuse into the plant tissue, solubilise the phytochemicals, and extract them (Capello, Fischer, & Hungerbühler, 2007; Nasrollahzadeh, Sajadi, & Khalaj, 2014). Thus, choosing the appropriate solvent is crucial for better outcomes. Water is one of the inexpensive, easily accessible, and harmless solvents (Sharghi, Khalifeh, & Doroodmand, 2009; Bose, Fatima, & Mereyala, 2003). Nonetheless, there are specific plant extracts that require other solvents such as methanol and ethanol (Duan, Wang, & Li, 2015; Varma, 2016). In terms of extract preparation, temperature has a discernible effect. At comparatively low temperatures, the phytochemicals' solubility will be hampered; at high temperatures, the phytochemicals will decompose. The optimal temperature range for extraction is between 60 ^{0}C and 80 ^{0}C (Seo, Lee, Elam, Johnson, Kang, & Arjmandi, 2014; Mohamad, Arham, Jai, & Hadi, 2014).

According to Zaabar, Aitout, Makhloufi, Belhamel, & Saidani, (2014); Kesavan, Gopiraman, & Sulochana, (2012); Gobara, Zaghloul, Baraka, Elsayed, Zorainy, Kotb, & Elnabarawy, (2017), there are two categories of green-based corrosion inhibitors: organic and inorganic. The synthetic materials that make up the organic family of environmentally safe corrosion inhibitors are not harmful to the environment. Scientific research on the inhibitory properties of natural products, such as peels, seeds, fruit shells, and leaves, which contain various organic compounds (such as amino acids, alkaloids, flavonoids, pigments, tannins, and so on) and suppress the dissolution reaction of metals and prevent environmental pollution, has increased in the interest of environmental protection (El-Enin, & Amin, (2015). Owing to their high productivity, the inorganic class of inhibitors is widely used in aqueous environments (Bethencourt, Botana, Calvino, Marcos, & Rodriguez-Chacon, 1998). To preserve both ferrous and non-ferrous metals, salts including sodium tungstate (Na_2WO_4), vandates ($NaVO_3$), nitrites ($NaNO_2$), silicates (Na_2Si2O_5), and chromates ($NaCrO_4$) were employed. Because they are hazardous, chromates and nitrites are being used less frequently. Although these compounds are quite costly, molybdate salts or rare earth metals have taken the role of chromates as corrosion inhibitors for open recirculating cooling water systems to safeguard the environment. The inorganic inhibitors, known as

phosphate salts, were frequently employed in conjunction with zinc salts (zinc ≤ 2 mg/L) to provide enhanced inhibitory efficacy (El-Enin & Amin, 2015).

II. GREEN CORROSION INHIBITORS

Eco-friendly or green corrosion inhibitors are naturally occurring substances that exhibit biological acceptability as inhibitors. These inhibitors can react appropriately to stop corrosion without endangering the environment's ecosystem. Because of the biological makeup of the plant, this type of inhibitor is typically extracted from it. Green inhibitors also include synthetic inhibitors that have no toxicity. Organic and inorganic green inhibitors are the two primary groups of environmentally beneficial or "green" inhibitors (Ahmed, Al-Mashhadani, Abdallh, Hussain, & Yousif, 2020). The first step in protecting against or limiting corrosion formation is to choose the right material depending on the application and final design. Second, the concentration of the inhibitor should be added if needed, and the ambient factors, pH level, temperature, and presence of active compounds should all be examined. Corrosion can also be prevented and controlled by insulating the material from the corrosive environment and making up for electrons lost by cathodic shielding. The most well-known technique for limiting, preventing, or regulating steel corrosion is the use of inhibitors. The inhibitory effects can be anodic, cathodic, or mixed, depending on the electrode treatment. It's also important to remember that some corrosion inhibitors are environment-specific and might not function in other situations (Varshney, Verma, Kumar, & Singh, 2023).

2.1 Theory of Green Corrosion Inhibitors

Gibbs' free energy has a direct bearing on the corrosion process. The rate of corrosion increases with negative Gibbs free energy. By building up on the surface of the corroded metals' active sites, inhibitors create a barrier that prevents further corrosion. The Pilling-Bedworth ratio, which determines the condition of the film surface, also controls the relative rate of corrosion. Insufficient oxide is created to protect the metal, rendering it non-protective, when the ratio is less than 1, that is, when the volume of the product generated by corrosion is less than that of the metal. The metal is protective when the ratio is more than 1, that is, when the volume of the product produced by corrosion is greater than the volume of metal; an excessively high ratio value, however, may cause breaking in the oxides that are created. The oxide becomes protective, and the metal and oxide have a good spatial fit when the ratio reaches 1 (Ahamed, Luqman, & Altalhi, 2021; Varshney et al., 2023). As per the adsorption process, some parameters, including the kind of electrolyte utilised, temperature, and the inhibitor's chemical makeup, might influence inhibition. It can create covalent connections for chemisorption. Green corrosion prevention is often carried out at room temperature, with temperature having an inverse relationship with anti-corrosion efficiency (Shehata, Korshed, & Attia, 2018; Ahamed, Luqman, & Altalhi, 2021; Varshney et al., 2023).

2.2 The Use of Environmentally Friendly Corrosion Inhibitors

Oguzie (2007) studied the inhibitive action of extracts of Sansevieria trifasciata leaf on aluminium corrosion in acidic media (2M HCl) and alkaline media (2M KOH), utilising the gasometric method. The extract adsorbs onto the aluminium surface, inhibiting the corrosion process by the Freundlich isotherm. The efficacy of this inhibition increased as the extracted content rose, but it reduced with an increase in temperature, indicating the behaviour of the physical adsorption mechanism. The study affirmed that the extract was an effective inhibitor in both settings. When halide additives were present, the inhibitory effectiveness was enhanced by synergistic actions.

Sultan, Areef, Abazeid, Khalil, Mahklouf, & Shushni (2022) studied the eco-friendly corrosion inhibition of Cynodon dactylon L. extract as an inhibitor of mild steel in saline solution. In a 3.5% NaCl solution, the extract of Cynodon dactylon L was tested for its ability to stop corrosion on mild steel. Using the gravimetric (Weight Loss) technique, the plant was extracted with 80% ethanol, and various concentrations were evaluated at temperatures between 30 ^{0}C and 60 ^{0}C and for immersion times between 4 and 72 hours. The outcomes demonstrated the high corrosion inhibition effectiveness (97.78%) of the Cynodon dactylon extract. The effectiveness of the Cynodon dactylon extract's inhibition rose as the extract concentration and immersion times increased, but it fell as the temperature increased. The plant's

presence of certain phytochemical substances that were adsorbed on the mild steel's surface may be the cause of the inhibitory action.

Hasan & Sisodia (2011) examined Paniala (Flacourtia jangomas) extract in 1M HCl and 0.5 H_2SO_4 solutions for the prevention of the corrosion of mild steel by using the weight loss technique at 30 ^{0}C. The study was carried out at 30 ^{0}C with and without the plant extract Flacourtia jangomas. It was demonstrated that the rate of corrosion was significantly lowered when an inhibitor was present. It was found that the concentration of the inhibitor affected the rate of corrosion. At 5% v/v inhibitor concentration, the greatest inhibition effectiveness (98%) for HCl was observed, and the inhibition efficiency showed little variation above this concentration. It was shown that 95% effectiveness was achieved at the same inhibitor concentration for 0.5M H_2SO_4. At lower inhibitor doses, the HCl medium showed better inhibition than the H_2SO_4 medium. The adsorption of Flacourtia jangomas was attributed to its chemical composition, which has been shown to contain a variety of substances, including tannins, phenolic compounds, steroids, and flavonoids, among others, and which have oxygen atoms with lone pair electrons for coordinate bonding with metal. The adsorption of plant extract was the reason for the decreased corrosion rate, based on the Langmuir and the Freundlich adsorption isotherms.

Velázquez-González, Gonzalez-Rodriguez, Valladares-Cisneros & Hermoso-Diaz (2014) investigated the efficiency of Rosmarinus officinalis as a corrosion inhibitor for 1018 carbon steel in 0.5 M H_2SO_4 using weight loss, potentiodynamic polarisation curves, and electrochemical impedance spectroscopy techniques at 25 ^{0}C. The hexane derivative exhibited an inhibitive efficiency, IE of 96%, but all the derivatives showed significant optimal qualities that inhibited corrosion. The extract containing hexanoic acid exhibited the greatest degree of efficacy. Using acetone, hexane, and methanol as the three extract solvents, inhibitor doses were added between 0 and 1000 ppm C. Studies have shown that Rosmarinus officinalis is a potent inhibitor of corrosion and that its potency increases with concentration. The flavonoid content of the extract improved the properties of the steel's passivating layer. The derivative's inhibitory qualities were regulated by the chemisorption system created by the adsorption free-energy value (-37.4 kJ.mol-1) and follow the Frumkin adsorption isotherm.

Al-Turkustani, Arab, & Al-Qarni (2011) investigated how water and alcohol compounds from the Medicago sativa plant may prevent mild steel corrosion in a 2 M sulphuric acid medium (H_2SO_4). In the chemical process, two analytical methods were employed: the mass-loss methodology and hydrogen evolution. The analytical behaviour was examined using potentiodynamic polarisation (PDP) and electrochemical impedance spectroscopy (EIS). It was discovered that the derivatives' mixed inhibitory behaviour mirrored the Langmuir adsorption isotherm. Furthermore, the main defence against corrosion was identified as chemical adsorption by charge transference between the inhibitor's molecules and the mild steel substrate.

Dehghani, Bahlakeh, Ramezanzadeh & Ramezanzadeh (2019) investigated the Citrullus lanatus fruit (CLF) extract in an aqueous medium for mild steel corrosion prevention using a combination of theoretical and experimental methods. About 91% Inhibition efficiency (IE) was shown to be caused by the O-H and C=C functional groups found in the phytochemicals, specifically riboflavin, citrulline, resveratrol, and hesperetin. The coordinated reaction was also demonstrated to be an essential protective factor. The SEM results demonstrated that mild steel created a smoother surface at higher concentrations of Citrullus lanatus (CL).

Ating, Umoren, Udousoro, Ebenso, & Udoh (2010) examined green corrosion inhibitors for aluminium in hydrochloric acid solutions using the leaves extract of Ananas sativum. Ananas sativum leaf ethanolic extract was investigated utilising weight loss and hydrogen evolution techniques. It was discovered that the plant extract prevented metal from corroding when exposed to acid. The effectiveness of inhibition increased with temperature and extract concentration. The optimal adsorption model for Ananas sativum's adsorption on an aluminium surface, according to adsorption studies, is the Langmuir adsorption isotherm. Temperature's impact on the inhibition and corrosion processes allowed for the evaluation of activation parameters, including activation energies (Ea), activation enthalpy (ΔH^o), and activation entropy (ΔS^o). In addition to supporting the suggested chemical adsorption, the values of Ea obtained in the presence of the extract were lower than those

obtained in the blank acid solution. The low and negative values of ΔGads that are produced demonstrate the spontaneity of the adsorption process.

Obot, & Obi-Egbedi (2010) using gasometric and thermometric methods at 30 and 60 °C, examined the leaf extracts of Chromolaena odorata L. (LECO) as a potential source of green inhibitor for the corrosion prevention of aluminium in 2 M HCl. The outcomes demonstrated how well the LECO worked to prevent aluminium from corroding in an acidic environment. Temperature harmed inhibition effectiveness, while extract concentration boosted it. The Langmuir adsorption isotherm and the adsorption of LECO on the Al surface were in agreement. They concluded that the ecologically friendly inhibitor may find use in surface coating and metal anodising processes in many sectors.

In Alvarez, Fiori-Bimbi, Neske, Brandan, & Gervasi's (2018) study, the weight loss measurements were used to examine the corrosion of mild steel in 1 M HCl with different concentrations of Rollinia extract or 0.007 g L−1 of either rolliniastatin-1 or motrilin. The temperature range of 24.85–54.85 ^{0}C was employed for weight loss measurements, and the results were utilised to compute the rate of corrosion and the effectiveness of inhibition. For the studied Carbon Steel in a 1 M HCl environment, it was discovered that the extract and the acetogenin solutions function as effective corrosion inhibitors. Furthermore, potentiodynamic polarisation tests show that both the two acetogenins under investigation and R. occidentalis function as mixed-type inhibitors. A Langmuir adsorption isotherm governs inhibitor adsorption. As the temperature and concentration of the extract increase, the effectiveness of inhibition diminishes. Spectroscopic examination indicates that the chemicals in the R. occidentalis extract and metal cations formed a complex.

Abiola, Otaigbe, & Kio (2009), using a chemical approach, studied the corrosion prevention capabilities of Gossypium hirsutum L. leaf and seed extracts (GLE and GSE) in 2 M NaOH solutions. Aluminium in the NaOH solution was not corroded by gossypium extracts. As the extract concentration increased, so did the efficacy of the inhibition. It was discovered that the leaf extract (GLE) worked better than the seed extract (GSE). At the maximum dose, the GSE showed 94% inhibitory efficiency, whilst the GLE gave 97%.

In Gobara, Zaghloul, Baraka, Elsayed, Zorainy, Kotb, & Elnabarawy (2017) study, a 0.5 M H_2SO_4 solution, extracted from Corchorus olitorius stems (ECS) was employed as a green inhibitor to prevent mild steel corrosion. The extract was subjected to both qualitative and quantitative examination using GC/MS. Potentiodynamic polarisation, weight loss, and electrochemical impedance spectroscopy were used to assess the extract's corrosion performance. The findings show that ECS is a mixed-type inhibitor with up to 93% inhibitory effectiveness that lowers both cathodic and anodic processes. To identify the features of inhibition, adsorption isotherm data were acquired at various temperatures and examined using specific adsorption isotherm models. Thermodynamic simulations demonstrated that when the temperature rises, the inhibition efficiency falls and increases with the concentration of the inhibitor. It was discovered that ECS adsorption on mild steel surfaces was exothermic and spontaneous. El-Awady's isotherm model suggests that adsorption is physisorption. Additionally, the corrosion findings were verified by examining the surface morphology using scanning electron microscopy (SEM).

Haldhar, & Prasad (2020) used weight loss, Tafel, and EIS, to study the corrosion inhibition of eucalyptus globulus (E. globulus) leaf extract on low carbon steel (LCS) in a 0.5 M sulphuric acid solution. At 600 mg/L, E. globulus exhibited the highest corrosion inhibition, with a value of 93.09%. Verification of the development of a protective layer on the surface of LCS is done using SEM and AFM. The existence of several functional groups comprising heteroatoms was established by FT-IR, while the adsorption phenomena were validated by UV-Vis spectroscopy. The Langmuir adsorption isotherm was followed by the inhibitory compounds' adsorption on the LCS surface.

A biodegradable and efficient extract from the leaves of Ficus tikoua was investigated by Wang, Tan, Bao, Xie, Mou, Li, Chen, Shi, Li, & Yang (2019) as a corrosion inhibitor for carbon steel in hydrochloric acid. The extract inhibitors function as a mixed-type with an inhibitory effectiveness of up to 95.8% at 24.85 ^{0}C, as observed from the electrochemical data. Additionally, this extract exhibits strong inhibitory efficacy throughout a broad temperature range, and

morphological examination further supported the related findings.

Saxena, Prasad, Haldhar, Singh, & Kumar, (2018) studied the corrosion inhibition impact of Saraca ashoka seeds extract, a plant that belongs to the Legume family, on mild steel corrosion in 0.5 M H_2SO_4 by the utilization of electrochemical impedance spectroscopy (EIS), potentiodynamic polarization, and weight loss techniques. The mild steel corrosion rate in an acidic solution is reduced by the epicatechin-containing extract. Using electrochemical and weight loss tests, the optimal inhibitory action of Saraca ashoka extract for mild steel in 0.5 M H_2SO_4 was found at 100 mg/L. Potentiodynamic polarization analysis indicates that the inhibitor could be a mixed kind. According to EIS evaluation, when inhibitors are present, the double-layer capacitance reduces and the charge transfer resistance rises.

Sun, Singh, Xu, Chen, Liu, & Lin (2017) used pomelo peel to make anti-corrosion compounds. The study examined N80 corrosion in 3.5-weight per cent NaCl saturated with CO_2 solution using the weight loss (WL) technique. The quantum chemical computation, FT-IR, SEM, SECM, and electrochemical techniques were used to study the process. The study demonstrated that physical adsorption was the predominant adsorption behaviour and that the procedure adhered to the Langmuir adsorption model's predictions. The extraction solution's ability to stop rusting increased with concentration and it achieved over 87% of the maximum efficiency. The results of quantum chemistry calculations indicate that the active ingredients that were separated from grapefruit peel have a good adsorption capacity.

Singh, Kumar, & Pramanik (2013) conducted a theoretical investigation of the effectiveness of a few plant extracts as a green corrosion inhibitor for mild steel in HCl solution, including Murraya koenigii, Andrographis paniculata, Terminalia arjuna, Citrus aurantium, Strychnosnux-vomica, Aegle marmelos, and Moringa oleifera. Among its strong phytochemical components are the aforementioned derivatives, which include brucine, andrographolide, mahabinine, sitosterol, arginine, pyrayafoline, skimmianine, and threonine. Numerous elements of the experimental configuration were examined, such as heteroatoms, the dipole moment, the lowest and highest occupied molecular orbitals, and the effect of Mulliken charges on the molecular capacity. The adsorption of adherent inhibitor molecules on the mild steel surface allowed the different plant derivatives to show sufficient shielding effectiveness. The results demonstrated that the inhibitor adsorption qualities are influenced by several factors, such as molecule size, the number of adsorption phases, the formation of metallic complexes, and the interface structure.

Wei, Heidarshenas, Zhou, Hussain, Li, & Ostrikov (2020) studied plant extracts from Auforpio turkiale, Azadirachta indica, Cassia occidentalis, Poinciana pulcherrima, papaya, and Calotropis Procera B. Of all these plants, Poinciana pulcherrima Cassia and Azadirachta indica demonstrated the greatest levels of effectiveness, at 96% and 98%, respectively. These substances inhibited the dissolution of the iron anodic reaction and the change in the hydrogen cathodic reaction by acting as mixed inhibitors on polarization curves. The study results indicated that mild steel protection may attain 96% efficiency. The assessment, which included electrochemical investigations, weight loss procedures, and SEM, revealed that these compounds were extremely cathodic inhibitors, satisfying the Langmuir adsorption isotherm. It was stated that the combined effect of many phytochemicals was a major element in the derivatives' optimum IE.

Eduok, Umoren, & Udoh (2012) assessed the stem and leaves of the Sida acuta plant for their capacity to halt the corrosion of mild steel in a 1 M sulphuric acid medium. Iodide ions were added to the medium to boost its inhibitory capacity. To evaluate shielding performance between 30 ^{0}C and 60 ^{0}C, two inhibitory mechanisms were used: weight loss and hydrogen evaluation measurements (HEMs). The leaves were found to have a peak inhibition of 85.25% despite having a similar pattern of inhibition (Freundlich adsorption isotherm), which was attributed to the leaves' greater phytochemical content.

In HCl environments, rubber leaf derivatives were investigated by Okewale, & Olaitan (2017) as mild steel corrosion inhibitors. Both the gravimetric system and FTIR were utilized to investigate the shielding behaviour. Anthraquinones, tannins, saponins, and flavonoids were among the phytochemicals in the derivatives that showed an 86% inhibitory activity. Furthermore, the Langmuir isotherm was followed by impulsive inhibitory

adsorption. Plant IE depends critically on the kinds and quantity of phytochemical alterations that occur at various phases.

Okafor, Ikpi, Uwah, Ebenso, Ekpe, & Umoren (2008) investigated the anti-corrosion characteristics of Phyllanthus amarus (Pa) extracts from the seeds (SD), leaves (LV), and combined leaves and seeds (LVSD) in sulphuric and HCl environments using weight reduction and gasometric techniques. The findings demonstrated that the derivatives acted as a shield in both media and that the inhibitory capacity rose with extract concentration. The temperature testing demonstrated that the rise in IE was caused by the rising temperature. However, as a result, the extract's activation energy dropped. The inhibitory performance is brought on by the extracts' chemical adsorption system on the metal surface. The Temkin isotherm was satisfied by the adsorption inhibitor's properties.

Okafor, & Ebenso (2007) conducted studies to evaluate the efficacy of several Carica papaya components as safe, non-toxic inhibitors of mild steel corrosion in H_2SO_4 at 300–600 ^{0}C, including leaves (LV), seeds (SD), heartwood (HW), and bark (BK). The plant derivatives were supplemented with organic and nitrogenous additions including choline, saponins, and other nitrogenous compounds. Gasometric and gravimetric methods were employed to determine the mechanism of inhibition of the different components. It was found that mild steel corrosion in H2SO4 was inhibited by the LV, SD, HW, and BK extracts. The inhibitory efficacies (IE) of the plant component extracts exhibit the following pattern: LV> SD> HW> 85% for BK or BK < 86% for HW < 94% for SD < 97.3% for LV. Temperature reduced the efficiency of inhibition, while extract concentration increased it. The physical adsorption of the plant's phytochemical components on the metal surface is thought to be the mechanism of inhibition. Both the Temkin and Langmuir adsorption isotherms were nicely supported by the experimental results.

2.3 Achievements of Green-Base Corrosion Inhibitors

The development of green corrosion inhibitors has led to more sustainable and ethical corrosion control methods in a variety of sectors, supporting international programmes aimed at resource and environmental conservation. Below are some of the achievements;

(I). Environmental Friendliness: Green corrosion inhibitors are often produced utilising environmentally friendly methods or from renewable materials. They are more environmentally friendly than traditional inhibitors since they are produced, used, and disposed of with less of an influence on the environment.

(II). Reduced Toxicity: Green corrosion inhibitors are either non-toxic or have far lower toxicity levels than many traditional corrosion inhibitors, which can include toxic components. This feature reduces health hazards related to inhibitor usage and improves workplace safety for those handling the inhibitors.

(III). Innovation and Research: The creation of environmentally friendly corrosion inhibitors has sparked creativity and investigation in the fields of materials engineering and corrosion science. Constant efforts are directed at enhancing the efficacy, compatibility, and affordability of green inhibitors, propelling ongoing developments in environmentally friendly corrosion prevention technology.

(IV). Cost-Effectiveness: Green corrosion inhibitors might occasionally cost more upfront than traditional inhibitors, but overall, they are usually more advantageous in the long run. Businesses can save money through decreased liability, waste management costs, and regulatory fines as a consequence of reduced environmental impact, enhanced safety, and regulatory compliance.

(V). Effectiveness: Green corrosion inhibitors may effectively prevent corrosion in a variety of metals and alloys, even though they are environmentally benign. On metal surfaces, they create protective layers that obstruct corrosion-causing processes, including oxidation and reduction reactions. A large number of green inhibitors work on par with or even better than conventional inhibitors.

(VI). Compatibility: Green corrosion inhibitors can be employed with various chemicals and additives that are often used in industrial processes, such as coatings, metalworking fluids, and cooling water treatment. Their interoperability allows them to be

easily integrated into current systems without requiring major changes or unfavourable interactions.

(VII). Biodegradability: Green corrosion inhibitors are made to gradually break down naturally, which lowers their environmental persistence and lowers the chance of long-term contamination. A crucial feature that complies with laws and policies that protect the environment is biodegradability.

2.4. Challenges of Green-Base Corrosion Inhibitors

In theory, it is better to utilise aqueous extracts rather than organic extracts since they include more polar phytochemicals that form strong bonds with metallic surfaces than the non-polar phytochemicals found in organic extracts. Plant extracts, whether aqueous or organic, are considered environmentally benign due to their biological origins; yet, at greater concentrations, they often show poor protective efficacy (Alrefaee et al., 2021)

(I) Poor Solubility
Because of their poor solubility in polar electrolytes, particularly at higher concentrations, organic extracts provide one of the largest hurdles when used as corrosion inhibitors (Alrefaee et al., 2021)

(II). Toxicity
Toxic solvents are often used in the manufacturing of organic extracts, and their release can harm the surrounding ecosystem, soil, and aquatic life (Alrefaee et al., 2021). It should be mentioned that a less dangerous extraction solvent should be utilised while extracting plant pieces (Varshney, Verma, Kumar, & Singh, 2023).

(III). Precipitation Issue
Practical observations have shown that organic extracts precipitate in polar electrolytes in the majority of situations (Alrefaee et al., 2021).

(IV) Short Lifespan
Their lifespan is one of the drawbacks. It is challenging to keep them for extended periods as the majority of them decompose naturally (Varshney et al., 2023).

(V). Labouring
Another drawback of employing plant extracts as corrosion inhibitors is their labour-intensive, multi-step production process (Alrefaee et al., 2021).

(VI). High Cost of Solvents
The majority of these solvents are expensive and may harm the extraction preparation's economics (Alrefaee et al., 2021).

III. BASIS OF ISOTHERM-ADSORPTION

Adsorption is the process that forms the basis of isotherms. Adsorption is the process by which molecular species gather at a material's surface as opposed to its bulk. The adsorbent is the substance on which adsorption occurs, while the adsorbate is the accumulating species. In essence, it is a surface phenomenon. Typically, the adsorbent is a solid surface, and the adsorbate is a gas (Vedantu, 01/05/2024). The adsorption mechanism and the interactions between the adsorbent and the adsorbate are shown by an adsorption isotherm (Kalam, Abu-Khamsin, Kamal, & Patil, 2021)

To create a theoretically modelable adsorption isotherm, a sequence of static adsorption tests with various surfactant concentrations can be carried out on the liquid-solid interface. The Henry model is the most basic adsorption isotherm, where the adsorbed quantity has a linear relationship with the bulk concentration of the adsorbate. Adsorption at lower concentrations, which is referred to as the Henry regime, is generally explained by this model. However, Langmuir was the first to present a coherent concept of homogeneous monolayer adsorption. Other adsorption isotherms, such as the Freundlich, Redlich–Peterson, Sips, Temkin, and others, are also documented in the literature and are used to fit data from static adsorption experiments. As seen in Figure 1, the adsorption isotherm's form may be divided into three groups: LS-shape (double plateau), S-shape (S-type), and L-shape (Langmuir). The monomolecular adsorption equation proposed by Langmuir helps explain the L-shape curve, a frequent adsorption isotherm for diluted solutions over a solid/liquid interface. The LS-shaped curve has two plateaus, while the S-shaped curve begins with a little slope and rises sharply (Kalam et al., 2021)

© NOV 2025 | IRE Journals | Volume 9 Issue 5 | ISSN: 2456-8880
DOI: https://doi.org/10.64388/IREV9I5-1712089

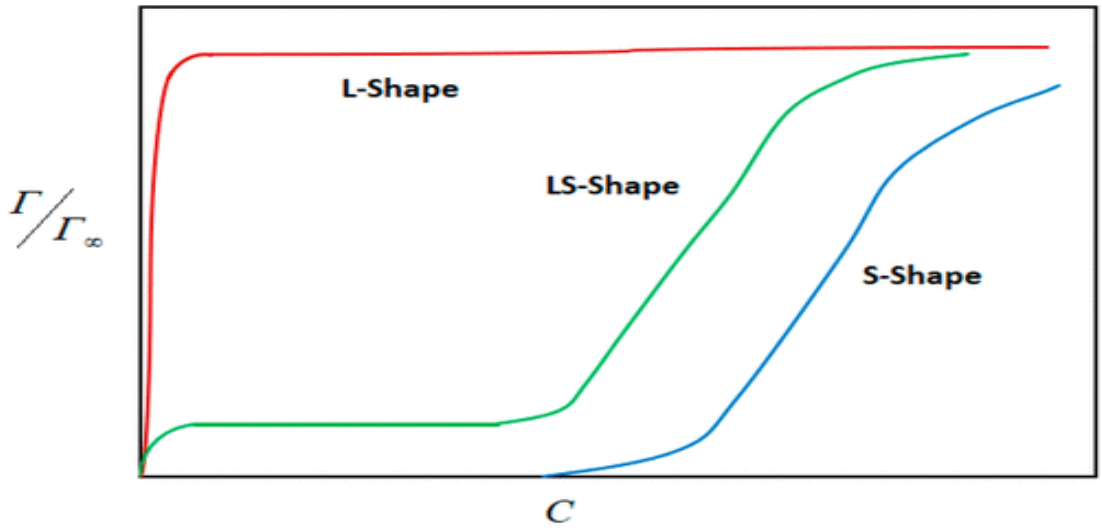

Figure 1: Adsorption isotherms in the L, S, and LS shapes. Adsorption and maximum adsorption are denoted by Γ and Γ∞, respectively, while the concentration is denoted by C. Reprinted by permission of ref (Source: Kalam et al., 2021)

3.1. Theories of Adsorption Isotherm

The two-step theory and the four-region theory are two well-known hypotheses that explain the process underlying adsorption isotherms. The next subsections go over those theories.

3.1.1. The Two-Step Theory

For L-type, S-type, and LS-type adsorption isotherms, Gu and Zhu developed two models (one-step and two-step); both models take adsorption as an interaction between surfactant molecules and vacant surface sites (Damacet, Hannouche, Gouda, & Hmadeh, 2024; Gu, & Zhu, 1990). In the one-step paradigm, an active site and a surfactant monomer interact to generate hemimicelles. Originally, the one-step model was created for the adsorption of nonionic surfactants on S-type curve-exhibiting silica gel (Kalam et al., 2021). Using the mass-action law, the one-step model's general mathematical form was created, as seen in equation 1:

$$\Gamma = \frac{\Gamma_\infty K C^n}{1+KC^n} \quad (1)$$

where n is the aggregation number, C is the surfactant concentration, k is the equilibrium constant, and Γ is the adsorption density, Γ_∞ is the adsorption density (maximum) at high concentration.

Adsorption occurs in two phases in the modified one-step model, known as the two-step model. First, by electrostatic contact, surfactant monomers are adsorbed on the solid surface at a concentration lower than the critical aggregation concentration (CAC). In the first phase, no aggregates are produced. It is demonstrated mathematically in equation 2:

$$\Gamma_1 = K_1 \Gamma_s C \quad (2)$$

where C is the concentration of surfactant monomers, Γ_s indicates the number of sites, k_1 is the equilibrium constant of the first step, and Γ_1 represents the quantity of adsorbed monomers.

3.1.2. The Four Region Theory

The most popular type of adsorption isotherm created for the adsorption of ionic surfactant on sites with opposing charges is the Somasundaran–Fuerstenau isotherm. This idea has been validated by electron spin resonance (ESR), Raman, and in situ fluorescence experiments. The adsorption isotherm is spread into four separate zones when plotted on a log-log scale, as Figure 2 illustrates. The following describes the chemistry of each location (Kalam et al., 2021).

© NOV 2025 | IRE Journals | Volume 9 Issue 5 | ISSN: 2456-8880
DOI: https://doi.org/10.64388/IREV9I5-1712089

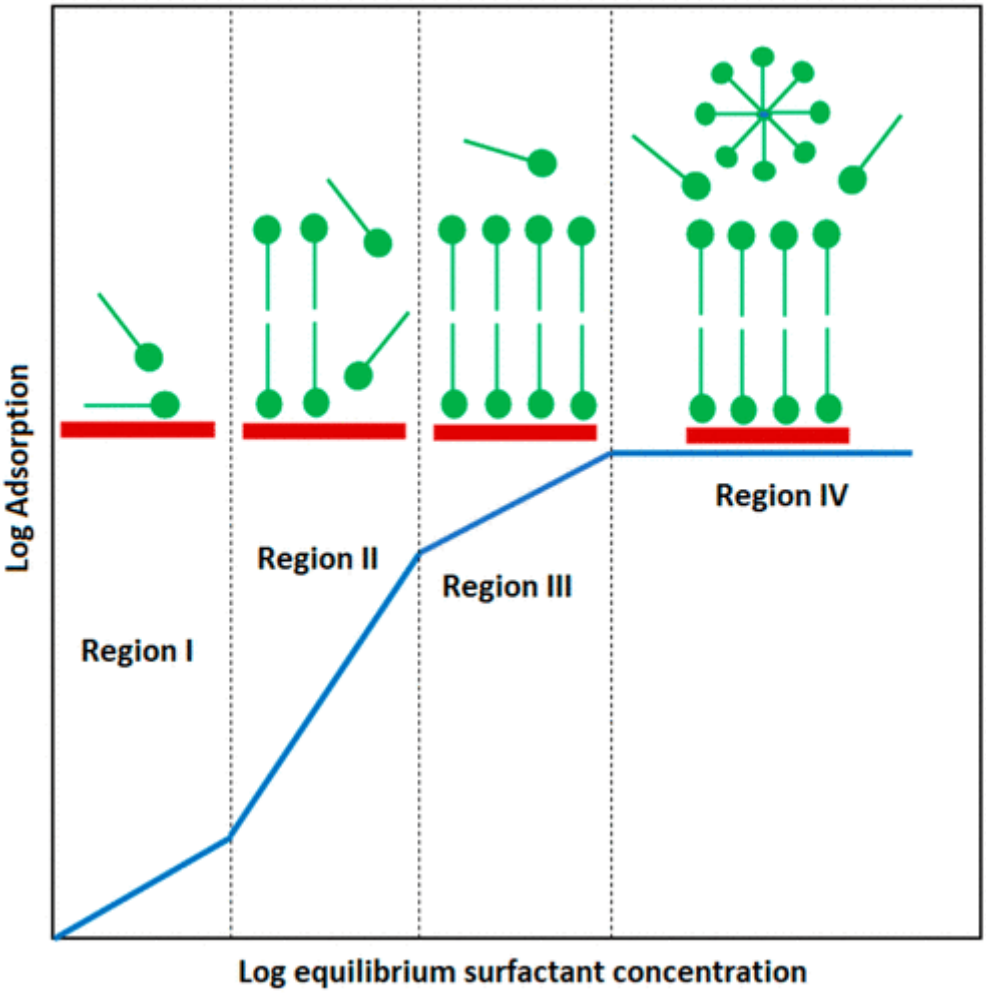

Figure 2: Typical surfactant adsorption isotherm illustration (Source: Kalam et al., 2021).

Region I is appropriate for modest adsorption densities and generally complies with Henry's law. Adsorption in this area is brought about by the electrostatic force of attraction between the surfactant ions and the charged surface. Adsorbed as monomers, surfactants do not interact with one another. Ionic strength conditions remain constant since the slope is unity.

Region II Here, the adsorption density increases dramatically. Here, aggregates such as hemimicelles and admicelles begin to develop as a result of the lateral interactions between hydrocarbon chains. Consequently, lateral associations and electrostatic attraction operate as the driving factors in this region, causing the slope of the isotherm to climb sharply. Hemicimole concentration (HMC) is related to the transition between regions I and II.

Region III Here, the isotherm's slope decreases when adsorption moves from region II to region III. Because surfactant ion adsorption has neutralised the solid surface in this area, electrostatic forces are not at work. Consequently, the adsorption isotherm's lower slope indicates that lateral attraction alone is the driving factor in this area.

Region IV is where the adsorption plateau is located. Micelles form, and the adsorption density stops varying when the surfactant concentration is at or above the critical micelle concentration (CMC). The lateral hydrophobic contact between hydrocarbon chains is the primary mechanism for adsorption, and the activity of the surfactant monomer remains constant. Typically, Region IV begins above the CMC.

3.2. Factors Affecting the Rate of Adsorption

Adsorption can be classified into two categories: chemical (chemisorption) and physical (physisorption). The former is caused by the formation of weak Vander Waal forces, while the latter is the result of the formation of chemical bonds. Adsorption rates can be affected by a variety of

© NOV 2025 | IRE Journals | Volume 9 Issue 5 | ISSN: 2456-8880
DOI: https://doi.org/10.64388/IREV9I5-1712089

factors, some of which can slow down the process, some of which can accelerate it, and different types of adsorptions can be affected differently by a given factor. The impact of a factor can be investigated by manipulating one of the variables while keeping the others unchanged (Vedantu, 01/05/2024)

1. Temperature:

In chemisorption, adsorption tendency first rises to a certain degree (due to an increase in the proportion of molecules containing activation energy) and subsequently drops. In physisorption, the adsorption tendency decreases with temperature owing to a decrease in attractive forces.

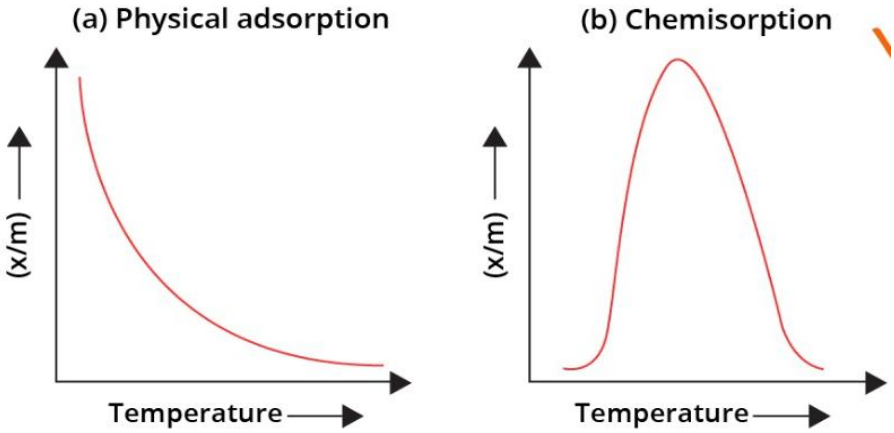

Figure 3: Variation of Extent of Adsorption (x/m) with Temperature) (Source:Vedantu, 01/05/2024)

2. Nature of Solid

This component is entirely dependent on the solid's surface area. The greater the solid's surface area, the greater the adsorption's extent. The order of adsorption for physisorption based on surface area is Piece of solid < Powdered solid < Sol of solid. Because of their empty valencies, the d and f block elements have a greater adsorption propensity in chemisorption.

3. Nature of Gas

A gas's adsorption propensity increases with its liquefaction tendency. One can infer a gas's liquefaction propensity by taking attractive forces into account. Increased liquefaction propensity and consequent adsorption of gas particles are directly correlated with higher attractive forces between them.

4. Pressure

The system's volume decreases as a result of gas adsorption. It follows that for a given temperature, the amount of adsorption should rise as the gas pressure increases. Isotherms are the curves that allow us to comprehend and calculate a mathematical relationship between the amount of adsorption and pressure at a certain temperature.

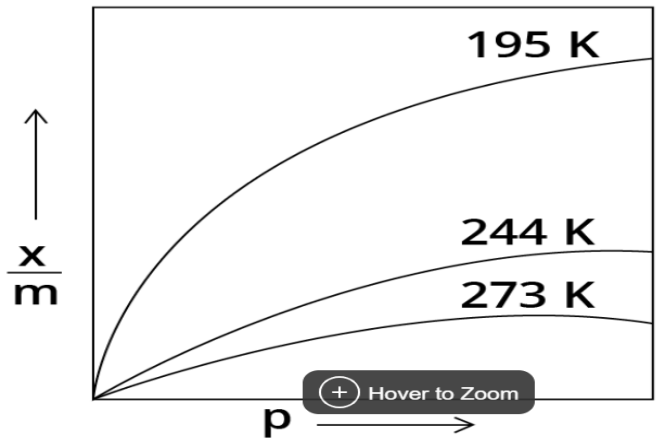

Figure 4: Variation of Extent of Adsorption (x/m) with Pressure (isotherm) (Source:Vedantu, 01/05/2024).

3.3 Adsorption Isotherm Models

Sorption is the broad term for the chemical-solid phase connection. In contrast to adsorption, which involves molecules adhering to a two-dimensional matrix, absorption involves molecules penetrating a three-dimensional matrix (Al-Ghouti, & Da'ana, 2020; Ehiomogue, Ahuchaogu, & Ahaneku, 2021). The process of adsorption is commonly referred to as chemisorption or physisorption, depending on how strongly the adsorbate and substrate interact. London forces, dipole-dipole forces, and van der Waals interactions are examples of weak electrostatic interactions that promote physisorption because they make it easy for the bands to break. On the other hand, chemisorption occurs when an electron is shared or transferred to create a covalent link between the adsorbate and the substrate. Compared to physisorption, the interactions in chemisorption are two orders of magnitude greater. Adsorbate forms a monolayer on the adsorbent in chemisorption, whereas a multilayer adsorbate forms on the adsorbent in physisorption. Reversible and occurring at low temperatures below the boiling point of the adsorbate, physical sorption has a low enthalpy. Chemisorption is an irreversible process that happens at all temperatures and has a high enthalpy. (Al-Ghouti, & Da'ana, 2020). The descriptive mechanism of the organic inhibitors' adsorption to the metal surface is provided by adsorption isotherm investigations (Akinbulumo, Odejobi, & Odekanle, 2020). Understanding the dependence relationship between adsorption tendency and all elements combined is challenging since adsorption depends on some variables, including temperature, pressure, surface area, and others. To investigate the impact on adsorption, all other parameters are held constant while one is altered. An isotherm graph is produced when the temperature is maintained at a steady level while the pressure is changed (Vedantu, 01/05/2024).

The isotherm illustrates the following relationship between pressure and adsorption:
I). Adsorption is directly correlated with pressure at low pressure.
II). Adsorption reaches saturation at high pressure, regardless(independent) of pressure.
III). Between the pressure conditions mentioned above, P^x influences adsorption, where $x<1$.
Two scientists, Irving Langmuir and Herbert Freundlich, attempted to extract a mathematical relation from the graph above.

This section covers some recent advances as well as the well-known adsorption isotherms.

3.3.1 One-Parameter Isotherm Model
3.3.1.1 Henry's Isotherm Model
It is the most fundamental adsorption isotherm and a one-parameter model. As shown by equation 3 suggests a linear relationship between the amount adsorbed and the bulk concentration of the adsorbate (Kalam et al., 2021).

$$q_e = K_{HE} C_e \quad (3)$$

Where q_e is the adsorbed amount at equilibrium in mg/g,

K_{HE} is the Henry's adsorption constant in L/g, and

C_e is the adsorbate's equilibrium concentration in mg/L.

A plot of q_e versus C_e produces a straight line, with a slope equal to K_{HE}.
When the adsorption sites' coverage ratio is low, Henry's model can be applied. Only at low solute concentrations does it roughly follow the data trend. Consequently, it exhibits monolayer adsorption at low adsorbate concentrations at first. In Region 1 of Figure 2, Henry's model is demonstrated. This basic model is not valid at high surfactant concentrations.

3.3.2 Two-Parameter Isotherm Models

3.3.2.1 Langmuir Isotherm Model
It is a more widely accepted isotherm (Vedantu, 01/05/2024). Although it was first created for gas-solid interaction, the Langmuir isotherm is now utilised for some adsorbents (Kalam et al., 2021). It assumes that the adsorbed gas is perfect and that it only forms a monolayer. It is therefore more appropriately applicable to chemisorption. In this case, the rate of adsorption is proportionate to the number of unoccupied sites, and all adsorption sites are regarded as equal. Additionally, it is assumed that the rates of adsorption and desorption are identical at equilibrium and that adsorption is reversible (Kalam et al., 2021; Vedantu, 01/05/2024).
The Langmuir isotherm can be expressed as follows under the following presumptions (Kalam et al., 2021; Shahbeig, Bagheri, Ghorbanian, Hallajisani, & Poorkarimi, 2013):
(a) Monolayer adsorption (One molecule makes up the adsorbed layer);

© NOV 2025 | IRE Journals | Volume 9 Issue 5 | ISSN: 2456-8880
DOI: https://doi.org/10.64388/IREV9I5-1712089

(b) Adsorption occurs in the adsorbent at particular homogenous locations.;
(c) Every site is the same and has the same energy;
(d) The molecules adsorbed on adjacent sites do not interact with one another.
(e) The adsorbent has a finite capacity for the dye (at equilibrium, a saturation point is reached where no further adsorption can occur);
(f) Once a dye occupies a site, no further adsorption can occur at that site;
(g) Adsorptional energy is constant and does not depend on the degree of occupation of an adsorbent's active center;
(h) The strength of the intermolecular attractive forces is thought to fall off rapidly with distance;
(i) The adsorbent has a uniform(homogeneous) structure.

$$q_e = \frac{q_o K_L C_e}{1+K_L C_e} \qquad (4)$$

where K_L is the Langmuir constant in L/mg, and q_o is the maximum quantity of adsorbed surfactant in mg/g. Equation 5's linearised version is

$$\frac{C_e}{q_e} = \frac{1}{K_L q_o} + \frac{C_e}{q_o} \qquad (5)$$

A plot between $\frac{C_e}{q_e}$ versus C_e will generate a straight line with a slope of $1 / q_o$ and an intercept equal to $1 / K_L q_o$.

Only one molecule can be adsorbed at each adsorption site under the monolayer assumption, which calls for identical adsorption sites. As soon as a surfactant molecule occupies a site, adsorption stops. At extremely low concentrations $K_L C_e \ll 1$, this model transforms into Henry's model.

The Langmuir isotherm model is shown by an L-shaped curve in Figure 3, which displays a single phase. The separation factor, also known as the equilibrium parameter, or R_L, is a crucial Langmuir model parameter that determines whether surfactant adsorption is favourable or unfavourable (Gunawardene, Gunathilake, Amaraweera, Fernando, Manipura, Manamperi, & Jayasinghe, 2021; Kalam et al., 2021). Mathematically, it can be represented as

$$R_L = \frac{1}{1+K_L C_o} \qquad (6)$$

Where, K_L and C_o are the Langmuir constant and the highest initial concentration of surfactant, respectively.
Positive adsorption is generally indicated by $R_L < 1$; irreversible adsorption is indicated by $R_L \sim 0$; a linear adsorption isotherm is shown by $R_L = 1$, and unfavourable adsorption is indicated by $R_L > 1$.

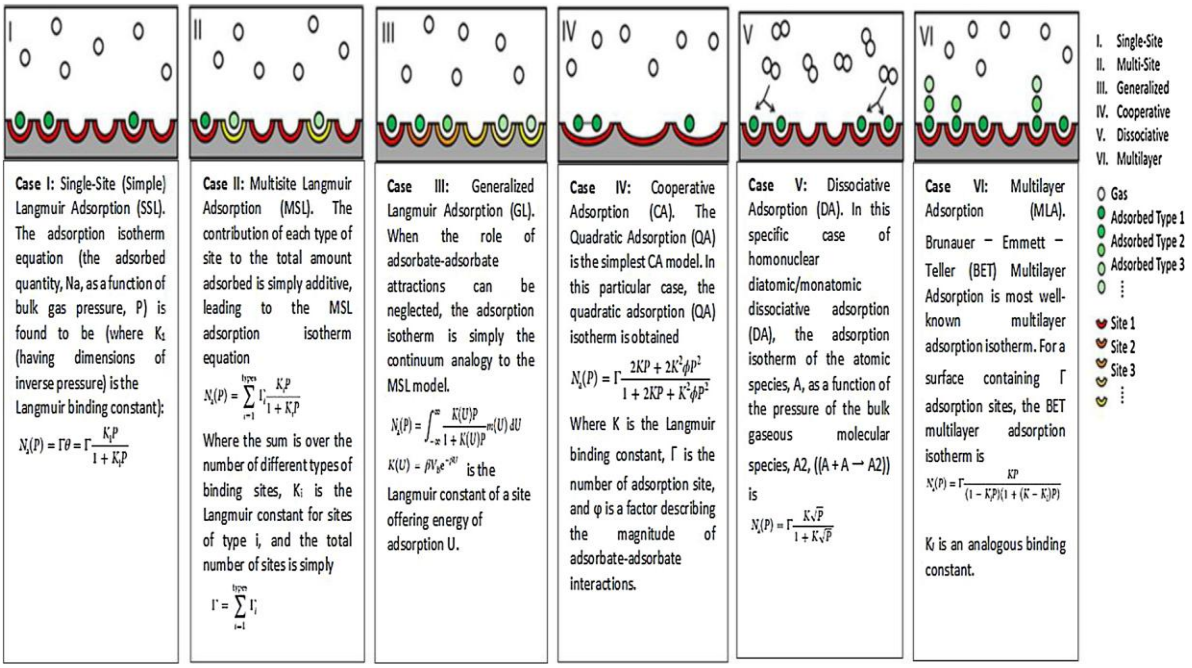

Figure 5: Schematic representation of Langmuir's six adsorption classifications, modified from (Source: Al-Ghouti, & Da'ana, 2020).

© NOV 2025 | IRE Journals | Volume 9 Issue 5 | ISSN: 2456-8880
DOI: https://doi.org/10.64388/IREV9I5-1712089

3.3.2.2 Freundlich Isotherm Model

The earliest known connection that describes non-ideal and reversible adsorption that is not limited to monolayer formation is the Freundlich isotherm (Foo, & Hameed, 2010). This empirical model can be applied to multilayer adsorption on heterogeneous sites, in contrast to the Langmuir isotherm. It is predicated on the nonuniformity of the affinities toward the heterogeneous surface and the dispersion of adsorption heat (Foo, & Hameed, 2010; Kalam et al., 2021). One way to display the mathematical model is

$$q_e = bC_e^{1/n} \qquad (7)$$

Where b is the adsorption capacity in L/mg, and 1/n is the adsorption intensity or surface heterogeneity. When 0 < 1/n < 1, adsorption is considered favourable. Unfavourable adsorption occurs when 1/n > 1 and is irreversible at 1/n = 1.

One way to express the linearised form is as

$$ln\, q_e = ln\, b + \frac{1}{n} C_e \qquad (8)$$

Plotting $ln\, q_e$ versus $ln\, C_e$ produces a straight line with a slope =1/n and intercept = ln b.

The linearised form is simple to understand. However, the linearization process produces propagating errors, leading to inaccurate parameter estimations. To calculate the model parameters, it is therefore advised to solve the nonlinear Freundlich model using nonlinear regression.

The energy distribution of adsorbed sites is assumed to decline exponentially, as described by the Freundlich isotherm for multilayer adsorption. It is not, however, applicable to a wide variety of adsorption data (Al-Ghouti, & Da'ana, 2020).

3.3.2.3 Temkin Isotherm Model

Hydrogen adsorption onto platinum electrodes in an acidic solution was first described using the Temkin empirical isotherm model, which is regarded as a chemisorption system (Al-Ghouti, & Da'ana, 2020). Although it disregards the extremely large and low concentration values, this isotherm model considers the interaction between the adsorbent and the adsorbate (Kalam et al., 2021; Al-Ghouti, & Da'ana, 2020; Vadi, Mansoorabad, Mohammadi, & Rostami, 2013; Al-Ghouti, & Da'ana, 2020)

According to this model, as surface coverage increases, the adsorption heat (ΔH_{ads}) of all molecules in the layer decreases linearly as a function of temperature rather than logarithmically (Vadi et al., 2020). There is only an intermediate concentration range for which this adsorption isotherm model is applicable (Al-Ghouti, & Da'ana, 2020; Shahbeig et al., 2013)

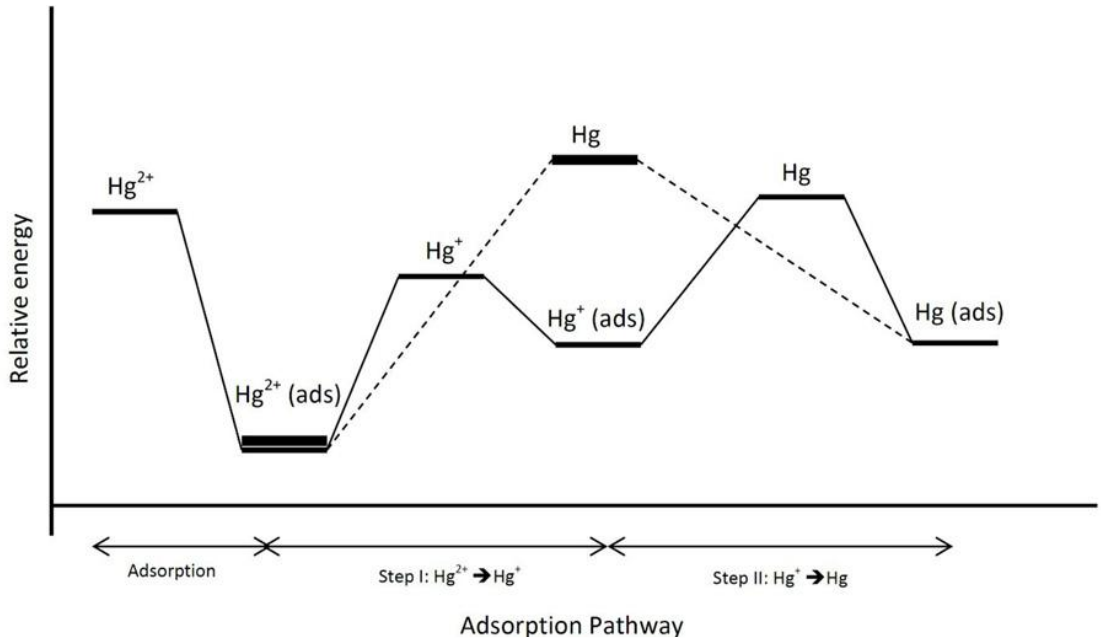

Figure 6: Adsorption pathways and relative energy profile of Hg^{2+} adsorption on the surface of adsorbent (Source: Al-Ghouti, & Da'ana, 2020)

Like the aforementioned isotherm models, the Temkin model's equation has both linear and non-linear variants. These are:

Non-linear form: $q_e = \frac{RT}{b_s} ln\, U_s\, C_e$ (9)

where R is the universal gas constant in J/(mol K), T is the temperature in K, b_s is the Temkin constant related to sorption heat in J/mol, and U_s is the Temkin isotherm constant in L/g.

The linearised form can be written as:

$$q_e = \frac{RT}{b_s} ln\, U_s + \frac{RT}{b_s} ln\, C_e \quad (10)$$

When plotting q_e against $ln\, C_e$, a straight line with a slope equal to $\frac{RT}{b_s}$ and intercept equal to $\frac{RT}{b_s} ln\, U_s$ is produced.

The Temkin model implies that the heat of adsorption of all molecules in the layer decreases linearly, rather than logarithmically, as the surface coverage rises (Kalam et al., 2021). If the gas phase's equilibrium does not need to be arranged in a densely packed structure with the same orientation, this model performs a great job of forecasting it. However, complicated adsorption systems, such as aqueous phase adsorption isotherms, cannot be represented by this isotherm model (Al-Ghouti, & Da'ana, 2020)

2.2.4.5 Dubinin-Radushkevich isotherm model
It is an empirical model that was first developed to explain how subcritical vapours might adsorb onto micropore materials through a process known as pore filling. The Dubinin-Radushkevich ssssadsorption isotherm model is typically employed to articulate the adsorption mechanism involving the Gaussian energy distribution onto heterogeneous surfaces. Although the model has a good track record of fitting data on high solute activity and the intermediate range of concentrations, its asymptotic properties are not sufficient, and it is unable to predict Henry's law at low pressure. (Al-Ghouti, & Da'ana, 2020; Ayawei, Ebelegi, & Wankasi, 2017; Foo, & Hameed, 2010). The method was typically used to differentiate between the chemical and physical adsorption of metal ions. By removing a molecule from its place in the sorption space to infinity, the mean free energy of the adsorbate, or E per molecule, can be calculated using the connection.

$$E = \left[\frac{1}{\sqrt{2B_{DR}}}\right] \quad (11)$$

where the isotherm constant is indicated by B_{DR}. In the interim, ε can be associated as follows:

$$\varepsilon = RT\, ln\left[1 + \frac{1}{C_e}\right] \quad (12)$$

where R, T, and C_e stands for the adsorbate equilibrium concentration (mg/L), absolute temperature (K), and gas constant (8.314 J/mol K), respectively.

The Dubinin-Radushkevich isotherm model is distinguished by its temperature dependence. Plotting adsorption data at various temperatures as a function of the logarithm of the amount adsorbed vs the square of potential energy reveals that all relevant data fall on the same curve, which is referred to as the characteristic curve (Foo, & Hameed, 2010).

2.2.4.6 Flory-Huggins Isotherm Model
The solution theory of the Flory-Huggins gives a straightforward but effective mathematical model for the thermodynamics of the polymer blends. According to this theory, solvent molecules occupy single sites whereas polymer segments occupy lattice sites. This entropy can be used to calculate the entropy of long-chain mixed compounds. (Al-Ghouti, & Da'ana, 2020). The Flory–Huggins isotherm model may convey the possibility and spontaneous nature of an adsorption process. It does this by periodically calculating the degree of surface coverage characteristics of adsorbate onto adsorbent (Al-Ghouti, & Da'ana, 2020; Foo, & Hameed, 2010).

Equations 13 and 14 represent the linear and non-linear equations for this adsorption isotherm model. By graphing log (θ/C$_o$) vs. log (1 – θ), their parameters can be found; the resulting straight line validates the model (Al-Ghouti, & Da'ana, 2020)

Linear form: $log\left(\frac{\theta}{C_o}\right) = log\, K_{FH} + n_{FH}\, log(1-\theta)$ (13)

Non-linear form: $\frac{\theta}{C_o} = K_{FH}(1-\theta)^{n_{FH}}$ (14)

In this context, n_{FH} is the number of metal ions that occupy the adsorption sites on two membranes, and θ is the surface coverage degree. Furthermore, the adsorption equilibrium constant is denoted by K_{FH}.

It is commonly employed for computing the spontaneous free Gibbs energy, given its relationship to the subsequent expression (Al-Ghouti, & Da'ana, 2020; Foo, & Hameed, 2010; Vijayaraghavan, Padmesh, Palanivelu, & Velan, 2006).

$$\Delta G^o = -RT\ ln(K_{FH}) \quad (15)$$

3.3.2.6 Hills Isotherm Model

This isotherm of adsorption provides an explanation for the binding of various species to homogenous substrates. With the adsorbates' capacity to attach at one site on the adsorbent, potentially impacting other binding sites on the same adsorbent, the isotherm model postulates that adsorption is a cooperative occurrence (Al-Ghouti, & Da'ana, 2020; Foo, & Hameed, 2010)

This adsorption isotherm model's original equation came from the nonideal competitive adsorption (NICA) isotherm. This isotherm model's linear and non-linear variants are expressed as follows (Al-Ghouti, & Da'ana, 2020):

Linear form: $log\left[\frac{q_e}{q_{SH}-q_e}\right] = n_H\ log\ C_e - log\ K_D$ (16)

Non-linear form: $q_e = \left[\frac{q_{SH}\cdot C_e^{nH}}{K_D + C_e^{nH}}\right]$ (17)

Additionally, in this model, binding has positive cooperativity when nH>1, negative cooperativity occurs when nH<1, and nH = 1 indicates hyperbolic or non-cooperative binding.

3.3.2.7 Halsey Isotherm Model

This adsorption isotherm assesses the multilayer adsorption system and provides a description of its condensation, at a considerable distance from the surface (Ehiomogue, Ahuchaogu, & Ahaneku, 2021; Al-Ghouti, & Da'ana, 2020; Ayawei, Ebelegi, & Wankasi, 2017), particularly for metal ions (Ehiomogue, Ahuchaogu, & Ahaneku, 2021). The Halsey model is appropriate for multilayer adsorption and heterogeneous surfaces where the adsorption heat is not uniformly distributed, much like the Freundlich isotherm model (Al-Ghouti, & Da'ana, 2020).

The Halsey equation's linearised form is as follows:

$$ln\ q_e = \left(\frac{1}{nH}\right) ln\ K_H - \left(\frac{1}{nH}\right) ln\ C_e \quad (18)$$

The following is the nonlinearized form (Al-Ghouti, & Da'ana, 2020).

$$q_e = e^{(ln\ K_H - ln\ C_e)/nH} \quad (19)$$

Plotting $ln\ q_e$ vs $ln\ C_e$ yields the Halsey isotherm parameters, where nH is acquired from the intercept and K_H from the slope.

3.3.2.8 Jovanovich Isotherm Model

With the potential addition of mechanical contact between the molecules that are adsorbing and desorbing, the assumptions of this model are essentially the same as those of the Langmuir isotherm model. The Jovanovich model's adsorption surface is taken into account, and although the equation for this adsorption isotherm model may be used for both mobile and monolayer localised adsorption without lateral interactions, it is less useful in physical adsorption (Al-Ghouti, & Da'ana, 2020; Ayawei, Ebelegi, & Wankasi, 2017; Ehiomogue, Ahuchaogu, & Ahaneku, 2021). When the concentration is large, the model's equation can reach the saturation limit; at low concentrations, it reduces to Henry's law. The Jovanovich equation approaches saturation more slowly than the Langmuir equation (Al-Ghouti, & Da'ana, 2020). The Jovanovich equation's linearised form is provided by

$$ln\ q_e = ln\ q_{max} - K_j C_e \quad (20)$$

The non-linearised form, however, is provided by

$$q_e = q_{max}\left(1 - e^{K_j C_e}\right) \quad (21)$$

Where, K_J is the Jovanovich constant (L/g), and q_{max} represents the maximal adsorbate uptake. These values can be determined by graphing lnq_e versus C_e (Al-Ghouti, & Da'ana, 2020).

The expression provides the generic Jovanovic equation for the homogeneous surface (Ehiomogue, Ahuchaogu, & Ahaneku, 2021).

$$q_e(P,T,e) = A[1 - exp(-bP)] \quad (22)$$

where A is the adsorption capacity at equilibrium and b is the Jovanovic parameter, which is defined by:

$$b = b_o exp\left(q/RT\right) \quad (23)$$

Where q is the isosteric heat of adsorption, and b_0 is the equivalent limiting value of b as the temperature approaches infinity (Ehiomogue, Ahuchaogu, & Ahaneku, 2021).

3.3.2.9 Volmer Isotherm Model

According to the Volmer isotherm model, adsorbed molecules are permitted to move about the surface of the adsorbent but are not permitted to interact with one another. The definition of the Volmer equation is Equation 24.

$$C_e = \frac{Q_v}{d(1-Q_v)} exp\left(\frac{Q_v}{1-Q_v}\right) \quad (24)$$

Where $Q_V\left(Q_V = {}^{q_e}/_{q_m}\right)$ is fractional coverage lying between zero and unity. d is the Volmer affinity constant, which relies on temperature. The factor $exp\left({}^{Q_V}/_{1-Q_V}\right)$ in the above equation accounts for the mobility of the adsorbate molecules (Saadi, Saadi, Fazaeli, & Fard, 2015)

3.3.2.10 Elovich Isotherm Model

The Elovich model, which depicts multilayer adsorption, is based on a kinetic concept and assumes that adsorption sites increase exponentially with adsorption. The formula for the Elovich isotherm model is Equation 25.

$$C_e = \frac{q_e}{q_{mE}K_E exp\left(\frac{-q_e}{q_{mE}}\right)} \quad (25)$$

3.3.2.10 Hill-Deboer Isotherm Model

A situation where there is both mobile adsorption and lateral contact among adsorbed molecules is described by the Hill-Deboer isotherm model (Ayawei, Ebelegi, & Wankasi, 2017; Saadi et al., 2015).

This is the Hill-Deboer isothermal model equation's linearised form (Ayawei, Ebelegi, & Wankasi, 2017)

$$ln\left[\frac{C_e(1-\theta)}{\theta}\right] - \frac{\theta}{1-\theta} = -ln\,K_1 - \frac{K_2\theta}{RT} \quad (26)$$

Where K_2 is the energy constant of the interaction between adsorbed molecules ($KJmol^{-1}$) and K_1 is the Hill-Deboer constant (Lmg^{-1}). Plotting $\ln[C_e(1-\theta)/\theta] - \theta/(1-\theta)$ versus θ can be used to analyse equilibrium data from adsorption studies (Ayawei, Ebelegi, & Wankasi, 2017)

While the non-linearised Hill-Deboer equation can be expressed as (Saadi et al., 2015)

$$C_e = \frac{\theta}{K_1(1-\theta)} exp\left[\frac{\theta}{1-\theta} - \frac{K_2\theta}{RT}\right] \quad (27)$$

where K_1 and K_2 stand for the adsorbate-adsorbent and adsorbate-adsorbate interactions, respectively. When the K_2 value is positive, adsorbed species are attracted to each other; when it is negative, the opposite is true. When there is attraction between the adsorbed species, the apparent affinity increases with loading; when there is repulsion, it decreases with loading. The Hill-de Boer equation reduces to the Volmer equation in the absence of any interaction between adsorbed molecules (i.e., K_2=0) (Saadi et al., 2015)

3.3.2.12 Fowler-Guggenheim Isotherm Model

This isotherm equation was proposed by Fowler-Guggenheim and accounts for the lateral interaction of the adsorbed molecules (Nandiyanto, Putri, Anggraeni, & Kurniwan, 2022; Dada, Ojediran, Okunola, Dada, Lawal, Olalekan, & Dada, 2019; Ayawei, Ebelegi, & Wankasi, 2017). One of the most straightforward correlations that enables prediction of the lateral interactions between adsorbates is the Fowler-Guggenheim isotherm model (Nandiyanto et al., 2022).

This isotherm model has the following linear form:

$$ln\left[\frac{C_e(1-\theta)}{\theta}\right] = -ln\,K_{FG} + \frac{2w\theta}{RT} \quad (28)$$

Where K_{FG} is the Fowler-Guggenheim equilibrium constant (Lmg^{-1}), θ is the fractional coverage, R is the universal gas constant ($KJmol^{-1}K^{-1}$), T is the temperature (k), and w is the interaction energy between adsorbed molecules ($KJmol^{-1}$). The premise of this isotherm model is that the heat of adsorption changes linearly with loading. Because of the increased interaction between adsorbed molecules as loading increases (i.e., w = positive), the heat of adsorption will increase with loading if the interaction between adsorbed molecules is attractive. On the other hand, the heat of adsorption falls with loading (that is, w = negative) if the interaction between the adsorbed molecules is repulsive. However, the Fowler-Guggenheim isotherm reduces to the Langmuir equation when $w = 0$, indicating that there is no interaction between adsorbed molecules (Ayawei, Ebelegi, & Wankasi, 2017; Farouq, &

Yousef, 2015; Saadi et al., 2015). The values for K_{FG} and w are obtained by plotting $ln[C_e(1-\theta)/\theta]$ versus θ. It is noteworthy that this particular model is only relevant in cases where the surface coverage is less than 0.6 ($\theta < 0.6$) (Ayawei, Ebelegi, & Wankasi, 2017)

3.3.2.13 Kiselev Isotherm Model

The localised monomolecular layer model, or Kiselev adsorption isotherm equation, is another name for it. only holds when the surface coverage $\theta > 0.68$ and the linearised expression is given as follows:

$$\frac{1}{C_e(1-\theta)} = \frac{K_1}{\theta} + K_i K_n \qquad (29)$$

Where K_n is the equilibrium constant of the formation of a complex between adsorbed molecules and K_i is the Kiselev equilibrium constant (Lmg−1). Plotting $^1/_{C_e(1-\theta)}$ versus $^1/_{\theta}$ equilibrium data from adsorption processes can be used to model (Ayawei, Ebelegi, & Wankasi, 2017)

3.3.3 Three-Parameter Isotherm Models

3.3.3.1 BET (Brunauer, Emmett and Teller) Isotherm Model

The theoretical isotherm equation Brunauer-Emmett-Teller is most useful when describing the equilibrium of gas-solid systems. The creation of the BET isotherm was used to create multilayer adsorption systems with relative pressures ranging from 0.05 to 0.30, which correspond to a monolayer coverage of 0.5–1.50. This approach is frequently used to calculate the surface area of an adsorbent using nitrogen adsorption data (Al-Ghouti, & Da'ana, 2020; Savran, Selçuk, Kubilay, & Kul, 2017; Saadi et al., 2015). BET linear form is expressed as follows:

$$\frac{C_e}{q_e(C_s-C_e)} = \frac{1}{q_m C_{BET}} + \frac{(C_{BET}-1)}{q_m C_{BET}} \frac{C_e}{C_s} \qquad (30)$$

where the energy of contact with the surface (L/mg), adsorbate monolayer saturation concentration (mg/L), and theoretical isotherm saturation capacity (mg/g) are explained by the BET adsorption isotherm constants C_{BET}, C_s, and q_m, respectively. From the plot of the linear $\frac{C_e}{q_e(C_s-C_e)}$ vs $\frac{C_e}{C_s}$, C_{BET} and q_m can be calculated from the intercept and slope, respectively. A negative value of C_{BET}, which measures the surface binding energy, suggests that the isotherm model is insufficient to explain the adsorption process (Savran et al., 2017).

It is possible to simplify the equation as both C_{BET} and $C_{BET}\left(^{C_e}/_{C_s}\right)$ are greater than 1:

$$q_e = \frac{q_s}{1-\left(\frac{C_e}{C_s}\right)} \qquad (31)$$

The liquid-solid interface is included in this concept, which is explained as follows:

$$q_e = \frac{q_{mBET} C_{BET} C_e}{(C_e-C_s)\left[1+(C_{BET}-1)\frac{C_e}{C_s}\right]} \qquad (32)$$

The BET model is regarded as a variant of the Langmuir model. It incorporates additional simplified assumptions, such as the following: the same adsorption energy is present in the second, third, and higher layers; these are the same assumptions used in the Langmuir model. Although the first layer's energy differs from the other layers, this energy is equivalent to the fusion heat that is unaffected by the interactions between the adsorbent and the adsorbate, and the number of layers tends to infinity as the concentration reaches the saturation concentration (Saadi et al., 2015). Utilising BET analysis, the surface area of porous materials like zeolites and metal-organic frameworks (MOFs) is typically ascertained.

MOFs are microporous materials with extremely large BET surface areas and surfaces that are anything but flat (Al-Ghouti, & Da'ana, 2020)

3.3.3.2 Redlich-Peterson Isotherm Model

The Redlich-Peterson isotherm has three parameters, combines the characteristics of the Freundlich and Langmuir isotherms, and has a hybrid adsorption process that deviates from ideal monolayer adsorption. Both homogeneous and heterogeneous systems can use this concept (Al-Ghouti, & Da'ana, 2020; Saadi et al., 2015). An exponential function exists in both the numerator and denominator of this isotherm model. Representing the equilibrium of the adsorption onto a broad range of concentrations, it has a linear relationship with the concentration. The numerator can approach the Henry area at infinite dilution since it originates from the Langmuir isotherm model. This isotherm model's linear and nonlinear equations are given by equations (33) and

(34), respectively (Al-Ghouti, & Da'ana, 2020; Foo, & Hameed, 2010).

$$ln\left[K_R\frac{C_e}{q_e}-1\right]=g\,ln(C_e)+ln(a_R) \qquad (33)$$

$$q_e=\frac{K_RC_e}{1+a_RC_e^g} \qquad (34)$$

By plotting $ln\left(\frac{C_e}{q_e}\right)$ versus $ln(C_e)$ makes it possible to calculate the values of g and a_R from the slope and intercept, respectively. When the adsorbate concentration in the liquid phase is high, this model reduces to the Friedrich equation.

$$q_e=\frac{K_R}{a_R}C^{1-\beta} \qquad (35)$$

Where, $K_R/a_R=K_F$ and $(1-\beta)=1/n$ of the Freundlich isotherm model. But when β=1, a_R=b, it reduces to the Langmuir equation (constant of Langmuir adsorption), and $K_R=bQ_o$ and it reduces to Henry's equation when $\beta=0$ (Al-Ghouti, & Da'ana,2020; Saadi et al., 2015), and Henry's constant is represented by $1/(1+b)$. To solve the equations, this isotherm model uses a minimized procedure. It optimises the coefficient of correlation between the experimental data points and the theoretical model's predictions. In terms of limitations, this model approaches the ideal Langmuir condition at the low concentration limit, where values of β are close to one, and it is consistent with the high concentration limit of the Freundlich isotherm model, where the exponent β tends to be zero (Al-Ghouti, & Da'ana, 2020).

3.3.3.3 Sips Isotherm Model

Sips created an equation that combines the Langmuir and the Freundlich isotherms by recognising the issue with the Freundlich equation's continual increase in the adsorbed amount with an increase in concentration. This results in an expression that, at a high enough concentration, shows a finite limit (N'diaye, & Kankou, 2020; Saadi et al., 2015; Behbahani, & Behbahani, 2014). Without adsorbate-adsorbate interactions, this model can be used to predict heterogeneous adsorption systems and localised adsorption (Al-Ghouti, & Da'ana, 2020; Saadi et al., 2015).

It reduces to the Freundlich isotherm at low adsorbate concentrations and predicts a monolayer adsorption capacity characteristic of the Langmuir isotherm at high concentrations. Generally speaking, changes in pH, temperature, and concentration are the primary factors influencing the equation parameters (Saadi et al., 2015; Foo, & Hameed, 2010). Because the Sips isotherm model reduces to the Freundlich model at low adsorbate concentrations, it defies Henry's law (Al-Ghouti, & Da'ana, 2020). The following linear and nonlinear expressions provide the Sips equation, respectively.

$$\beta_s\,ln(C_e)=-ln\left(\frac{K_s}{q_e}\right)+ln(a_S) \qquad (36)$$

$$q_e=\frac{q_sa_SC_e^{Bs}}{1+a_SC_e^{Bs}} \qquad (37)$$

Values close to (or exactly) 1 indicate a solid with relatively homogeneous binding sites; if Bs is unity, the Langmuir equation applicable for ideal surfaces is recovered. The constant Bs is frequently regarded as the heterogeneity factor, and the system heterogeneity could stem from the solid, the adsorbate, or a combination of both. The Bs parameter is usually greater than unity, and therefore, the larger this parameter, the more heterogeneous the system (Saadi et al., 2015).

The Sips Isotherm Model parameters are pH, temperature, and concentration-dependent, and isotherm constants differ by linearization and nonlinear regression (Al-Ghouti, & Da'ana, 2020; Ayawei, Ebelegi, & Wankasi, 2017)

3.3.3.4 Harkins-Jura Isotherm Model

The Harkin-Jura isotherm model postulates that absorbents with heterogeneous pore distribution may experience multilayer adsorption on their surface. The Harkins-Jura isotherm model equation is expressed as;

$$\frac{1}{q_e^2}=-\left(\frac{B}{A}\right)log\,C_e \qquad (38)$$

where A and B are Harkins-Jura constants that can be obtained by plotting $\frac{1}{q_e^2}$ versus $log\,C_e$ (Ayawei, Ebelegi, & Wankasi, 2017)

The presence of a heterogeneous pore distribution can account for the strong fit of adsorption data using Harkins-Jura, similar to the Halsey equation at high concentrations. While the BET theory is a useful tool for assessing an adsorbent's surface area, the Harkins-

Jura isotherm is another technique that can be used to calculate surface area (Saadi et al., 2015).

Saadi et al., (2015). In reference to earlier research [Gürses, Karaca, Doğar, Bayrak, Açıkyıldız, & Yalçın, 2004, and Shanavas, Kunju, Varghese, & Panicker, 2011], Harkins-Jura provides the most accurate match with equilibrium data when it comes to multilayer adsorption isotherm models with three parameters.

3.3.3.5 Toth Isotherm Model

Another empirical adjustment to the Langmuir equation that aims to lower the discrepancy (error) between experimental data and the projected value of equilibrium data is the Toth isotherm. The heterogeneous adsorption systems that meet the low and high-end boundaries of the adsorbate concentration are best described by this model. (Ayawei, Ebelegi, & Wankasi, 2017; Behbahani, & Behbahani, 2014). This isotherm model is typically used to describe heterogeneous adsorption systems, meeting both low and high adsorbate concentration requirements. The correlation of this isotherm model assumes an asymmetrical quasi-Gaussian distribution of energy, where the majority of sites have lower adsorption energy than the peak or mean value (Al-Ghouti, & Da'ana, 2020). The Toth isotherm model is expressed as follows (Ayawei, Ebelegi, & Wankasi, 2017)

$$\frac{q_e}{q_m} = \theta = \frac{K_e C_e}{[1+(K_L C_e)^n]^{1/n}} \qquad (39)$$

Where K_L and n are Toth isotherm constants (mg g^{-1}). This equation reduces to the Langmuir isotherm equation when n = 1. Thus, the heterogeneity of the adsorption system is characterised by the parameter n, and the system is considered heterogeneous if it deviates further from unity (1). The Toth isotherm can be rearranged in the following ways to provide a linear form (Ayawei, Ebelegi, & Wankasi, 2017)

$$ln\frac{q_e^n}{q_m^n - q_e^n} = n\,ln\,K_L + n\,ln\,C_e \qquad (40)$$

Sigma Plot software can be utilised to analyse the parameters of the Toth model through a nonlinear curve fitting method.

The sorption isotherm data of the biosorption of nickel (II) ions onto Sargassum wightii were better characterised by the Toth model than by the other three-parameter models (Redlich–Peterson, sips, Khan, and Radke–Prausnitz) based on the correlation coefficient, RMSE, and chi-square test (Vijayaraghavan et al., 2006).

3.3.3.6 Koble-Carrigan Isotherm Model

The Koble-Carrigan isotherm model is a three-parameter equation that combines the Langmuir and the Freundlich isotherms that are used to depict or represent equilibrium adsorption data (Ayawei, Ebelegi, & Wankasi, 2017; Behbahani, & Behbahani, 2014). Usually, heterogeneous adsorption surfaces are employed with this model (Shahbeig, Bagheri, Ghorbanian, Hallajisani, & Poorkarimi, 2013). The Koble-Carrigan isotherm equation is given as:

$$q_e = \frac{AC_e^n}{1+BC_e^n} \qquad (41)$$

An optimisation technique based on trial and error (equation 42) is used to get the isotherm constants, A, B, and n, from the linear plot (Behbahani, & Behbahani, 2014), and the parameters can also be evaluated using an add-in function of Microsoft Excel (Ehiomogue, Ahuchaogu, & Ahaneku, 2021; Ayawei, Ebelegi, & Wankasi, 2017).

$$\frac{1}{q_e} = \frac{1}{A} + \frac{1}{C_e^n} + \frac{B}{A} \qquad (42)$$

According to Han, Zhang, Zou, Shi, & Liu, (2005), It has been shown that the Koble-Carrigan isotherm best fits the data when it comes to using grain chaff to remove lead ions from aqueous solutions (Ehiomogue, Ahuchaogu, & Ahaneku, 2021). This model reduces to a Freundlich isotherm at large adsorbate concentration. Only when the constant "n" is bigger than or equal to one is it valid. Despite a high concentration coefficient or low error value, the model is unable to describe the experimental data when "n" is less than unity (1) (Ayawei, Ebelegi, & Wankasi, 2017).

3.3.3.7 Khan Isotherm Model

For pure solutions, the Khan isotherm is a generalised model that can represent both extremes—Langmuir and the Freundlich types. It was created for adsorption systems with many components as well as those with just one (Al-Ghouti, & Da'ana, 2020; Saadi et al., 2015). For pure component adsorption isotherms, the generalised equation is written as:

$$q_e = \frac{q_s b_K C_e}{(1+b_K C_e)^{a_K}} \qquad (43)$$

Where a_K is Khan isotherm model exponent, q_s is Khan isotherm maximum adsorption capacity (mg g^{-1}), and b_K is the Khan isotherm model constant (Ayawei, Ebelegi, & Wankasi, 2017; Vijayaraghavan et al., 2006). High correlation coefficients are associated with well-defined maximum uptake values, minimum chi-square values, and sum square error (ERRSQ) values (Al-Ghouti, & Da'ana, 2020; Saadi et al., 2015; Behbahani, & Behbahani, 2014). The Khan model reduces to the Freundlich isotherm at large values of equilibrium concentration (C_e). However, when a_K equals unity, this isotherm model reduces to the Langmuir isotherm system (Al-Ghouti, & Da'ana, 2020; Saadi et al., 2015).

3.3.3.8 Radke-Prausnitz Isotherm Model

By adding a new coefficient to the Langmuir equation, Radke and Prausnitz suggested a minor adjustment that enhanced the fit of their experimental results. This model's three isotherms can be computed using the following equations: 44, 45, and 46 (Saadi et al., 2015)

$$q_e = \frac{q_{mI} K_I C_e}{(1+K_I C_e)^{m_I}} \qquad (44)$$

$$q_e = \frac{q_{mII} K_{II} C_e}{1+K_{II} C_e^{m_{II}}} \qquad (45)$$

$$q_e = \frac{q_{mIII} K_{III} C_e}{1+K_{III} C_e^{m_{III}^{-1}}} \qquad (46)$$

Where q_m is Radke-Prausnitz maximum adsorption capacity (mg g^{-1}), m is Radke-Prausnitz model exponent, and K is Radke-Prausnitz equilibrium constant (Ayawei, Ebelegi, & Wankasi, 2017). This isotherm model lowers to a linear isotherm at low adsorbate concentration, turns into the Freundlich isotherm at high adsorbate concentration, and transforms into the Langmuir isotherm at m = 0. This isotherm's ability to provide a satisfactory match over a large range of adsorbate concentrations is another noteworthy feature. The parameters of the Radke-Prausnitz model are determined using a nonlinear statistical fit of the experimental data (Ayawei, Ebelegi, & Wankasi, 2017). Most often, low adsorbate concentration adsorption systems employ the Radke-Prausnitz isotherm model (Ehiomogue, Ahuchaogu, & Ahaneku, 2021)

The Radke–Prausnitz model does not well correlate with the nickel biosorption data, as indicated by significant RMSE and chi-square values (Vijayaraghavan et al., 2006).

3.3.3.9 Jossens Isotherm Model

The distribution of the energy of adsorbate-adsorbent interactions on adsorption sites is the basis of the Jossens isotherm model. The model assumes that the adsorbent surface is heterogeneous concerning the interactions between adsorbate and adsorbent (Ehiomogue, Ahuchaogu, & Ahaneku, 2021; Ayawei, Ebelegi, & Wankasi, 2017; Saadi et al., 2015). The Jossens model equation is written as:

$$C_e = \frac{q_e}{H} exp(F q_e^u) \qquad (47)$$

Where F and H are temperature-dependent. At low capacity, this equation can be reduced to Henry's law (Saadi et al., 2015). u is Jossens' isotherm constant, and it is a property/characteristic of the adsorbent regardless of the adsorbent's nature and temperature (Ayawei, Ebelegi, & Wankasi, 2017). At low capacity, the equation reduces to Henry's law. But after reorganising, the linearised Jossens equation is given (Ehiomogue, Ahuchaogu, & Ahaneku, 2021; Ayawei, Ebelegi, & Wankasi, 2017).

$$ln\left(\frac{C_e}{q_e}\right) = -ln(H) + F q_e^p \qquad (48)$$

The values of F and H can be obtained from either the plot of $ln\left({C_e}/{q_e}\right)$ versus q_e or by using the least square fitting procedure.

3.3.3.10 Unilan Isotherm Model

Another empirical equation that results from assuming a uniform distribution of energy is the Unilan isotherm model. The Langmuir local isotherm and uniform distribution are the sources of the term "Unilan." Both at low and high concentration, the Unilan equation fits the experimental data quite well (Saadi et al., 2015; Do, 1998). The Unilan equation is given:

$$q_e = \frac{q_{mU}}{2s} ln\left[\frac{1+re^{s} C_e}{1+re^{-s} C_e}\right] \qquad (49)$$

The system's heterogeneity is determined by the parameters; the more heterogeneous the system, the larger the parameter. The isotherm approaches irreversible behaviour when the value of s approaches approximately 10. When s=0, the Unilan equation

reduces to the classical Langmuir equation because the range of the energy distribution is zero.

3.3.3.11 Frumkin Isotherm Model

The interaction between the adsorbed species was described by the development of the Frumkin isotherm equation. Equation 50 presents the Frumkin correlation (Saadi et al., 2015).

$$C_e = \frac{\theta}{K_f(1-\theta)} exp(-f\theta) \quad (50)$$

The equation, as mentioned earlier, reduces to the Langmuir isotherm if f=0, or when there is no interaction between the adsorbate species.

3.3.3.12 Fritz-Schlunder (III) Isotherm Model

Fritz and Schlunder suggested an empirical relation with three-parameter isotherm models to represent the equilibrium data. The Fritz-Schlunder model is shown in Equation 51 (Saadi et al., 2015).

$$q_e = \frac{q_{mFS} K_{FS} C_e}{1+q_m C_e^{m_{FS}}} \quad (51)$$

3.3.3.13 McMillan-Teller (MET) Isotherm Model

Surface tension effects in the BET isotherm led to an extension of the MacMillan-Teller (MET) isotherm model (Saadi et al., 2015). The definition of the MET equation is:

$$q_e = q_{SM} \left[\frac{K}{ln\left(\frac{C_s}{C_e}\right)}\right]^{1/3} \quad (52)$$

The approximate value of the logarithmic term when Cs/Ce approaches unity is:

$$q_e = q_{SM} \left(\frac{KC_e}{C_s - C_e}\right)^{1/2} \quad (53)$$

Fitting experimental data to this empirical isotherm is possible at relative concentrations greater than 0.8. The BET isotherm, however, is accurate for relative concentrations less than 0.4 (Saadi et al., 2015)

3.3.3.14 Frankel-Halsey-Hills (FHH) Isotherm Model

A modified form of the BET mode is called the Frenkel-Halsey-Hill (FHH). Multilayer adsorption is described by the Frenkel-Halsey-Hill (FHH) adsorption isotherm, which assumes that the adsorption potential varies with the distance from the surface of the adsorbent to the adsorbed molecule layer. The effects of surface heterogeneity on the adsorption of molecules in the second and higher adsorbed layers are ignored by the BET model for the case of heterogeneous surfaces. However, the FHH model assumes that surface heterogeneity influences adsorption in every adsorbed layer (Al-Ghouti, & Da'ana, 2020; Saadi et al., 2015). The FHH adsorption isotherm can be found using Equation 54.

$$q_e = \left[\frac{-1}{A_{FHH}} ln\left(\frac{C_e}{C_s}\right)\right]^{\frac{-1}{B_{FHH}}} \quad (54)$$

Long-range van der Waals interactions between the surface and the initial adsorbed molecule layer are specified by $A_{FHH,}$ as are interactions between nearby adsorbate molecules that provide details on the surface's adsorption capacity. Higher A_{FHH} values, for example, suggest that more adsorbate might be adsorbed. The interactions between the surface and ensuing adsorbate layers are described by BFHH (Saadi et al., 2015). The most homogenous sample has a value of 2.95, while the least heterogeneous sample has a value of 2.69. This parameter increases from 2.55 for the most heterogeneous sample (Al-Ghouti, & Da'ana, 2020; Saadi et al., 2015). B_{FHH} for van der Waals forces equals 3, and about 2.7 is the typical value for an adsorbent observed in practice (Do, 1998). Greater surface heterogeneity or smaller B_{FHH} values show that the adsorbent continues to have an effect on adsorbed molecules at increasing distances from the surface (Saadi et al., 2015). The Harkins-Jura equation becomes relevant when the adsorption energy decreases with the second power of the distance from the interface, as seen by the FHH equation's reduction to the Harkins-Jura equation when B_{FHH} = 2 (Do, 1998).

3.3.3.15 Aranovic Isotherm Model

This equation is comparable to the Aranovich isotherm, which is a modified form of the BET isotherm (Saadi et al., 2015). The term (1 - P/Po) in the denominator of the two equations has a different exponent. The exponent in the Aranovich instance is one-half, whereas it is one in the BET example (Do, 1998). Equation 55 is the multimolecular Aranovich equation.

$$q_e = \frac{q_{mAr} C_{Ar} \frac{C_e}{C_s}}{\left(1-\frac{C_e}{C_s}\right)^{1/2}\left(1+C_{Ar}\frac{C_e}{C_s}\right)} \quad (55)$$

Aranovich asserted that the BET equation's narrow validity range (relative pressure of 0.05 to 0.4 (Do,

1998), relative concentration of 0.02 to 0.4 (Saadi et al., 2015)) and that his isotherm accurately reflects the limiting instances. Additionally, the denominator of the BET equation contains a component of (1-P/PO), which provides infinite spreading pressure at saturation pressure (Do, 1998).

His model is predicated on the following: (1) The adsorbent surface is uniformly flat. (2) A lattice model can be applied to the phase in contact with the adsorbent, which is a vacancy solution. (3) Only the configurational components of the free energy are taken into consideration. (4) The energy shift that occurs when a molecule evaporates depends on the number of layers.

3.3.3.16 Red Head Isotherm Model

This model's range of validity is extended to larger concentration ranges employing the Redhead isotherm, which spans the multilayer adsorption region. The Red Head isotherm equation is given as;

$$q_e = q_{mR} \cdot \left[\frac{(2n_R-2)\cdot C_e}{C_s-C_e}\right]^{1/n_R} \qquad (56)$$

where nR is the empirical parameter; most of the time, it was found to be between 2.5 and 4.5. The Redhead equation is located in the upper range of the decreased concentration, below the BET equation, just like the Aranovich equation (Saadi et al., 2015; Do, 1998)

3.3.3.17 O'Brien and Myers (OBMR) Isotherm Model

O'Brien and Myers developed an equation (OBMR) that considers the heterogeneity of adsorption surfaces. This expression is based on the Langmuir isotherm. The Langmuir equation is represented by the first term in the bracket of the OBMR isotherm, and the second term expresses the correction resulting from the effects of adsorbent heterogeneity. The parameter n represents the variance of the adsorption energy distribution. Like the Toth and UNILAN equations, this isotherm equation is a three-parameter model that may reasonably describe a wide range of experimental data (Chilev, Dicko, Langlois, & Lamari, 2022; Do, 1998)

$$Q = Q_{max}\left[\frac{bf}{1+bf} - \frac{n^2(1+bf)}{2(1+bf)^3}\right] \qquad (57)$$

Where f stands for gas fugacity

3.3.3.18 Potential Theory (PT) Isotherm Model

The hypothesis of micropore filling explains this kind of adsorption mechanism. This hypothesis is extremely helpful when it comes to adsorption in microporous materials like activated carbons. Generally speaking, microporous adsorbents with a high specific surface area are employed in the adsorption process of purifying hydrogen. Under these circumstances, the micropore filling technique is appropriate. Thermodynamics explains the differences between the two mechanisms. When surface layering occurs, the adsorbent's chemical potential is unaffected by the amount adsorbed, but when micropore filling occurs, the chemical potential is reliant on the amount adsorbed. This model (PT) is given by the equation (58), and the molar work of adsorption, also known as the adsorption potential, is the essential quantity in the micropore filling and is provided by equation (59) (Chilev et al., 2022)

$$W = W_{max}\left[-\left(\frac{RT\,ln\left(\frac{f_s}{f}\right)}{b}\right)^n\right] \qquad (58)$$

$$A = RT\,ln\left(\frac{f_s}{f}\right) \qquad (59)$$

where f_s is the free liquid's saturation vapour fugacity. The molar energy unit is used for the adsorption potential A. This energy is known as the characteristic energy since it is unique to a certain gas/solid system. The parameter, which differs from the interaction energy in the Langmuir equation, indicates the strength of the adsorbate–adsorbent interaction. The interaction energy is a measurement of the interaction between an adsorbate molecule and the surface quantity, and the Langmuir mechanism is related to monolayer-type adsorption. The characteristic energy of micropore filling is the result of an interaction between the adsorbent and the amount of adsorbate inside the micropore. This is the application of the basic adsorption theory equation:

$$\theta = f\left(A/_{b,n}\right) \qquad (60)$$

where θ is the percentage of the adsorbate's micropore volume that is occupied. The parameter linked with the distribution function, n, is considered to be the function, f, which is the distribution function of the filling of micropores θ over the differential molar work of adsorption (Chilev et al., 2022)

3.3.4 Four Parameter Isotherm Models

3.3.4.1 Fritz-Schlunder (IV) Isotherm Model

Fritz and Schlunder expanded the four-parameter isotherm model of a different Langmuir-Freundlich type empirically (Saadi et al., 2015). This model equation is given as;

$$q_e = \frac{C C_e^{\alpha}}{1+D C_e^{\beta}} \qquad (61)$$

This formula holds when ∝ and β ≤ 1. This model reduces to the Freundlich equation at large adsorbate liquid-phase concentrations. The model reduces to the Langmuir equation for ∝=β=1 (Saadi et al., 2015)

3.3.4.2 Dubinin-Astakhov Isotherm Model

The surface heterogeneity of the adsorbent is described by the Dubinin-Astakhov isotherm model. Nonetheless, several empirical findings verify that this model is capable of explaining adsorption in a nearly uniform microporous environment. The equation of Dubinin-Astakhov is given by equation (61); (Saadi et al., 2015)

$$\theta_{DA} = exp\left(\frac{-A_D}{E_A}\right)^{n_D} \qquad (62)$$

$$A_D = RT\, ln\left(\frac{C_S}{C_e}\right) \qquad (63)$$

Where n_D describes the surface heterogeneity

3.3.4.3 Baudu isotherm Model

To reduce errors in determining the Langmuir constant and coefficient from the isotherm's gradient and tangent across a larger concentration range, the Baudu isotherm model was created (Ehiomogue, Ahuchaogu, & Ahaneku, 2021). The Langmuir coefficients, q_{mL} and b, are not constants throughout a large concentration range, according to the computation of the coefficients using the measurement of tangents at the various equilibrium concentrations. Equations 64 and 65 represent their concentration variations (Al-Ghouti, & Da'ana, 2020; Ayawei, Ebelegi, & Wankasi, 2017; Saadi et al., 2015).

$$b = b_0 C_e^{x} \qquad (64)$$

$$q_{mL} = q_{mB} C_e^{y} \qquad (65)$$

Plotting $ln(q_{mL})$ and $ln(b)$ against $ln(C_e)$ yields the model's parameters, b_0, q_{mB}, x and y. The Langmuir equation has been changed into the Baudu isotherm model, or equation (66)

$$q_e = \frac{q_{mB} b_0 C_e^{(1+x+y)}}{1+b_0 C_e^{(1+x)}} \qquad (66)$$

where d0 is the equilibrium constant, y is the Baudu parameter, x is the Baudu parameter, and qmB is the Bauder maximum adsorption capacity (mg g−1) (Ehiomogue, Ahuchaogu, & Ahaneku, 2021; Ayawei, Ebelegi, & Wankasi, 2017). This formula holds when (1+x+y) and (1+x) < 1. The Freundlich equation is the model's reduced form for lesser surface coverage (Al-Ghouti, & Da'ana, 2020; Saadi et al., 2015).

3.3.4.4 Weber-van Vliet Isotherm Model

As a four-parameter isotherm model, the Weber-van Vliet equation was put forth to forecast this model's behaviour using equilibrium data (Saadi et al., 2015). This model equation is given as;

$$C_e = P_1 q_e^{\left(P_2 q_e^{P_3} + P_4\right)} \qquad (67)$$

where the isotherm parameters are P1, P2, P3, and P4. Using a multiple nonlinear curve fitting technique, which is based on the minimisation of the residual's sum of squares, one can find the isotherm parameter (Al-Ghouti, & Da'ana, 2020)

3.3.4.5 n-Layer BET Isotherm Model

The maximum n-layers that can be adsorbed onto the interior surface, according to the n-layer BET isotherm, is assumed. When the adsorption layer is constrained by n layers, or when the adsorption space is confined in the case of finite pore sizes (Saadi et al., 2015; Do, 1998). The n-Layer BET model equation is given as;

$$q_e = \frac{q_{m,nBET} C_{nBET} C_e}{C_s - C_e} \cdot \frac{1-(n_{BET}+1)\left(\frac{C_e}{C_s}\right)^{n} + n_{BET}\left(\frac{C_e}{C_s}\right)^{n_{BET}+1}}{1+(C_{nBET}-1)\left(\frac{C_e}{C_s}\right) - C_{nBET}\left(\frac{C_e}{C_s}\right)^{n_{BET}+1}} \qquad (68)$$

where C_{nBET} is the BET adsorption constant is linked to the energy of interaction with the surface.

Equation (68) reduces to the standard BET equation when n approaches infinity. When $n_{BET} = 1$, the equation is transformed to the Langmuir equation. The first layer's heat of adsorption is higher than the heat of fusion, meaning that the attractive interactions between the adsorbed molecule and the adsorbent are

stronger than those between molecules in the liquid state. This explains why the value C_{nBET} is typically greater than 1 (Saadi et al., 2015; Do, 1998).

3.3.4.6 Guggenheim Anderson de-Boer (GAB) Isotherm Model

The Langmuir and BET physical adsorption isotherms are modified to form the Guggenheim Anderson de-Boer (GAB) isotherm. The criterion for the difference in standard chemical potential between the molecules in the second and subsequent adsorption layers and those in the liquid state is K_G, which is inevitably included in this isotherm (Saadi et al., 2015). The GAB equation by;

$$q_e = \frac{q_{mG} C_{GAB} K_G C_e}{(C_s - K_G C_e)[1+(C_{GAB}-1)]K_G \frac{C_e}{C_s}} \qquad (69)$$

where K_G and C_{GAB} are the GAB constants, which correspond to the interaction energies between the molecules that have been sorbed at each unique sorption site. The heat of adsorption of the second layer and any succeeding layers is less than the heat of fusion when the K_G parameter is typically less than unity. However, the heat of adsorption of the second layer is the same as the upper layers (Saadi et al., 2015).

The following equation is valid when:

$$q_{mBET} < q_{mG} \qquad C_{BET} > C_{GAB}$$

On the other hand, Equation (65) becomes the BET equation if K_G=1; consequently

$$C_{BET} = C_{GAB} \qquad C_{BET} = C_{GAB}$$

The heat of fusion is equal to the heat of adsorption of the second and higher layers, according to the BET isotherm.

3.3.4.7 Anderson (IV) Isotherm Model

Another version of the BET equation is the Anderson (IV) adsorption isotherm, which makes the assumption that the adsorbent's structure is such that only a finite number of layers are permitted to absorb adsorbate, meaning that each succeeding layer's surface area for adsorption is reduced. (Saadi et al., 2015). The equation of this isotherm is given as;

$$q_e = \frac{q_{mAn,4} C_{An,4} C_e}{(C_s - jC_e)\left[1+(C_{An,4}-1)\frac{C_e}{C_s}\right]} \qquad (70)$$

where j is the portion that is accessible in the layer that follows. Within every layer, this portion is taken to be constant. This equation reduces to the Langmuir equation at j=0 and yields the well-known BET equation at j=1

3.3.4.8 Dubinin-Serpinsky Isotherm Model

Dubinin and Serpinsky proposed an equation explaining water adsorption by active carbons. It is predicated on the idea that adsorption starts at what are known as primary sites and that hydrogen bonds are formed at these hydrated sites to facilitate more adsorption. This formula is an enhanced rendition of a previous explanation (Saadi et al., 2015), and it can be shown as:

$$C_e = \frac{C_s q_e}{C_{DS}(q_0+q_e)(1-K_{DS}q_e)} \qquad (71)$$

The decrease in acting adsorption centres with increased micropore filling is taken into consideration by the term $(1 - K_{DS}q_e)$. The requirement that the amount adsorbed at the saturated concentration will equal the maximal adsorption capacity establishes the value of the parameter K_{DS}.

3.3.4.9 Marczewski-Jaroniec Isotherm Model

Another name for the Marczewski-Jaroniec isotherm is the four-parameter general Langmuir equation. It is advised based on the local Langmuir isotherm's assumption and the adsorption energies in the active sites on the adsorbent (Ayawei, Ebelegi, & Wankasi, 2017). Here is how the isotherm equation is expressed:

$$q_e = q_{MMJ}\left[\frac{(K_{MJ}C_e)^{nMJ}}{1+(K_{MJ}C_e)^{nMJ}}\right]^{M_{MJ}/n_{MJ}} \qquad (72)$$

Where M_{MJ} and n_{MJ} are characteristics describe the adsorbent surface's heterogeneity, M_{MJ} describes the distribution spreading in the direction of greater adsorption energy, whereas the distribution spreading in the direction of lower adsorption energies is described by n_{MJ}.

When n_{MJ} and M_{MJ} = 1, the isotherm simplifies to the Langmuir isotherm; when $n_{MJ} = M_{MJ}$, it reduces to the Langmuir-Freundlich model.

3.3.5 Five Parameter Isotherm Model

3.3.5.1 Fritz-Schlunder (V) Isotherm Model

The application of the Fritz-Schlunder isotherm model, a five-parameter model, can examine an

extensive range of experimental equilibrium data. Higher complexity nonlinear regression techniques are needed to solve this problem (Al-Ghouti, & Da'ana, 2020; Ayawei, Ebelegi, & Wankasi, 2017; Saadi et al., 2015). The Fritz-Schlunder equation is given by;

$$q_e = \frac{1 m^{FS} S_S K_1 C_e^{\alpha_{FS}}}{1 + K_2 C_e^{\beta_{FS}}} \qquad (73)$$

This model decreases to the Frisch isotherm model at larger adsorbate concentrations, although it approaches the Langmuir isotherm model when α_{FS} and β_{FS}=1.

3.3.5.2 Anderson (V) Isotherm Model

Another modified form of the BET adsorption isotherm is the five-parameter model known as the Anderson (V) equation. Combining the GAB and the Anderson (IV) isotherm models increases the relative concentration range of the BET model. This occurs when the surface area of a layer that is available for adsorption is smaller than the layer that comes before it, and the heat of adsorption of the second layer and above is less than the heat of fusion (Saadi et al., 2015). Combining equations (69) and equation (70) gives rise to equation (77), which is the Anderson (V) equation;

$$q_e = \frac{q_{mAn,5} C_{An,5} K_A C_e}{(C_S - j K_A C_e)\left[1 + (C_{An,5} - 1) K_A \frac{C_e}{C_S}\right]} \qquad (77)$$

3.4 Adsorption Thermodynamics

An essential component of the study of adsorption is adsorption thermodynamics, which is crucial for determining the adsorption mechanism (physisorption and chemisorption) (Tran, Lima, Juang, Bollinger, & Chao, 2021; Sahmoune, 2019). The standard change in Gibbs free energy (ΔG°) can be simply derived from Equation (78) using the laws of thermodynamics.

$$\Delta G° = -RT \ln K \qquad (78)$$

where T is the temperature (K), K is the equilibrium constant, and R is the universal gas constant (8.314 J mol−1 K−1) (Milonjić, 2007).

Rearranging equation (78), we have: (Tran et al., 2021)

$$K = \exp\left(\frac{-\Delta G°}{RT}\right) \qquad (79)$$

The link between the ΔG° parameter and the others (ΔH° and ΔS°), assuming that they are temperature-independent, is expressed as follows (Tran et al., 2021)

$$\Delta G° = \Delta H° - T\Delta S° \qquad (80)$$

An adsorption process that is both feasible and spontaneous has a negative Gibbs free energy value. Substituting equation (78) into equation (80), we have: (Sahmoune, 2019).

$$\ln K = -\frac{\Delta H°}{RT} + \frac{\Delta S°}{R} \qquad (81)$$

While the enhanced randomness at the solid/solution interface is reflected by the positive value of change in entropy (ΔS°), the positive value of change in enthalpy (ΔH°) indicates that the adsorption is an endothermic process (Sahmoune, 2019).

IV. CONCLUSION

The search for environmentally safe and sustainable corrosion inhibitors offers a viable solution to the problems associated with corrosion control. Green corrosion inhibitors must be used to reduce the harmful consequences that conventional corrosion control techniques have on the environment and human health.

Our exploration of the principles underlying green corrosion inhibition has revealed the diverse mechanisms by which these inhibitors operate, including passivation, adsorption, and film formation. Understanding these mechanisms is crucial for designing novel inhibitors with enhanced performance and selectivity, tailored to specific corrosion environments and materials.

Through thorough studies into new inhibitor formulations, synthesis pathways, and performance assessments, the research aims to enhance the area of green corrosion inhibition.

REFERENCES

[1] Abiola, O. K., Otaigbe, J. O. E., & Kio, O. J. (2009). Gossipium Hirsutum L. Extracts as Green Corrosion Inhibitor for Aluminum in NaOH Solution. Corrosion Science, 51(8), 1879-1881.

[2] Ahmed, W. A., Al-Mashhadani, M. H., Abdallh, M., Hussain, Z., & Yousif, E. (2020). Eco-friendly green corrosion inhibitors in overview. Research Journal in Advanced Sciences, 1(1), 1-16.

[3] Akinbulumo, O. A., Odejobi, O. J., & Odekanle, E. L. (2020). Thermodynamics and adsorption study of the corrosion inhibition of mild steel by Euphorbia heterophylla L. extract in 1.5 M HCl. Results in Materials, 5, 100074.

[4] Al-Ghouti, M. A., & Da'ana, D. A. (2020). Guidelines for the use and interpretation of adsorption isotherm models: A review. Journal of hazardous materials, 393, 122383.

[5] Alrefaee, S. H., Rhee, K. Y., Verma, C., Quraishi, M. A., & Ebenso, E. E. (2021). Challenges and advantages of using plant extract as inhibitors in modern corrosion inhibition systems: Recent advancements. Journal of Molecular Liquids, 321, 114666. Journal of Molecular Liquids, 321, 114666. https://doi.org/10.1016/j.molliq.2020.114666

[6] Al-Turkustani, A. M., Arab, S. T., & Al-Qarni, L. S. S. (2011). Medicago Sative Plant as Safe Inhibitor on the Corrosion of Steel in 2.0 M H2SO4 Solution. Journal of Saudi Chemical Society. 15 (1), 73–82. doi: 10.1016/j.jscs.2010.10.008

[7] Alvarez, P. E., Fiori-Bimbi, M. V., Neske, A., Brandan, S. A., & Gervasi, C. A. (2018). Rollinia Occidentalis Extract as Green Corrosion Inhibitor for Carbon Steel in HCl Solution. Journal of industrial and engineering chemistry, 58, 92-99.

[8] Anees, A.K., & Khalid, W.H. (2012). Prevention of Steel Corrosion by Cathodic Prevention Techniques. International Journal of Chemical Technology, 4(1), 17-30. Doi:10.3923/ijet.2012.17.30

[9] Ating, E.I., Umoren, S.A., Udousoro, I.I., Ebenso, E.E., & Udoh, A.P. (2010). Leaves extract of Ananas Sativum as Green Corrosion Inhibitor for Aluminium in Hydrochloric Acid Solutions. Green Chemistry Letters and Reviews, 3(2), 61-68, DOI: 10.1080/17518250903505253

[10] Ayawei, N., Ebelegi, A. N., & Wankasi, D. (2017). Modelling and interpretation of adsorption isotherms. Journal of Chemistry, 2017.

[11] Behbahani, T. J., & Behbahani, Z. J. (2014). A new study on asphaltene adsorption in porous media. Petroleum and Coal, 56(5), 459-466.

[12] Bethencourt, M., Botana, F. J., Calvino, J. J., Marcos, M., & Rodriguez-Chacon, M. A. (1998). Lanthanide Compounds as Environmentally-Friendly Corrosion Inhibitors of Aluminium Alloys: a review. Corrosion Science, 40(11), 1803-1819.

[13] Bose, D. S., Fatima, L., & Mereyala, H. B. (2003). Green chemistry approaches to the synthesis of 5-alkoxycarbonyl-4-aryl-3, 4-dihydropyrimidin-2 (1 H)-ones by a three-component coupling of one-pot condensation reaction: Comparison of ethanol, water, and solvent-free conditions. The Journal of organic chemistry, 68(2), 587-590.

[14] Capello, C., Fischer, U., & Hungerbühler, K. (2007). What is a green solvent? A comprehensive framework for the environmental assessment of solvents. Green Chemistry, 9(9), 927-934.

[15] Chemat, F., Vian, M. A., & Cravotto, G. (2012). Green Extraction of Natural Products: Concept and Principles. International Journal of Molecular Sciences, 13(7), 8615-8627. https://doi.org/10.3390/ijms13078615

[16] Chilev, C., Dicko, M., Langlois, P., & Lamari, F. (2022). Modelling of single-gas adsorption isotherms. Metals, 12(10), 1698.

[17] Dada, A. O., Ojediran, J. O., Okunola, A. A., Dada, F. E., Lawal, A. I., Olalekan, A. P., & Dada, O. (2019). Modeling of biosorption of Pb (II) and Zn (II) ions onto PaMRH: langmuir, freundlich, temkin, dubinin-raduskevich, jovanovic, flory-huggins, fowler-guggenheim and kiselev comparative isotherm studies. International Journal of Mechanical Engineering and Technology (IJMET), 10(2), 1048-1058.

[18] ssDamacet, P., Hannouche, K., Gouda, A., & Hmadeh, M. (2024). Controlled Growth of Highly Defected Zirconium–Metal–Organic Frameworks via a Reaction–Diffusion System for Water Remediation. ACS Applied Materials & Interfaces.

[19] Dehghani, A., Bahlakeh, G., Ramezanzadeh, B., Ramezanzadeh, M. (2019). A Combined Experimental and Theoretical Study of Green Corrosion Inhibition of Mild Steel in HCl Solution by Aqueous Citrullus Lanatus Fruit (CLF) Extract. Journal of Molecular Liquids.

279, 603–624. doi:10.1016/j.molliq.2019.02.010

[20] Do, D. D. (1998). Adsorption analysis: Equilibria and kinetics (with cd containing computer MATLAB programs) (Vol. 2). World Scientific.

[21] Duan, H., Wang, D., & Li, Y. (2015). Green chemistry for nanoparticle synthesis. Chemical Society Reviews, 44(16), 5778-5792.

[22] Eduok, U. M., Umoren, S. A., & Udoh, A. P. (2012). Synergistic Inhibition Effects Between Leaves and Stem Extracts of Sida Acuta and Iodide Ion for Mild Steel Corrosion in 1 M H2SO4 Solutions. Arabian Journal of Chemistry. 5 (3), 325–337. doi:10.1016/j.arabjc.2010.09.006

[23] Ehiomogue, P., Ahuchaogu, I. I., & Ahaneku, I. E. (2021). REVIEW OF ADSORPTION ISOTHERMS MODELS. Acta Technica Corviniensis-Bulletin of Engineering, 14(4).

[24] El-Enin, S. A., & Amin, A. (2015). Review of corrosion inhibitors for industrial applications. Int. J. Eng. Res. Rev, 3(2), 127-145.

[25] El-Etre, A. (2008). Inhibition of C-steel corrosion in acidic solution using the aqueous extract of zallouh root. Materials Chemistry and Physics, 108(2-3), 278-282. https://doi.org/10.1016/j.matchemphys.2007.09.037

[26] Farouq, R., & Yousef, N. S. (2015). Equilibrium and kinetics studies of adsorption of copper (II) ions on natural biosorbent. International Journal of Chemical Engineering and Applications, 6(5), 319.

[27] Foo, K. Y., & Hameed, B. H. (2010). Insights into the modeling of adsorption isotherm systems. Chemical engineering journal, 156(1), 2-10.

[28] Gobara, M., Zaghloul, B., Baraka, A., Elsayed, M., Zorainy, M., Kotb, M. M., & Elnabarawy, H. (2017). Green corrosion inhibition of mild steel to aqueous sulfuric acid by the extract of Corchorus olitorius stems. Materials Research Express, 4(4), 046504.

[29] Gu, T., & Zhu, B. Y. (1990). The S-type isotherm equation for adsorption of nonionic surfactants at the silica gel—water interface. Colloids and surfaces, 44, 81-87.

[30] Gunawardene, O. H. P., Gunathilake, C. A., Amaraweera, A. P. S. M., Fernando, N. M. L., Manipura, A., Manamperi, W. A., ... & Jayasinghe, J. A. S. C. (2021). Removal of Pb (II) ions from aqueous solution using modified starch. Journal of Composites Science, 5(2), 46.

[31] Gürses, A., Karaca, S., Doğar, Ç., Bayrak, R., Açıkyıldız, M., & Yalçın, M. (2004). Determination of adsorptive properties of clay/water system: methylene blue sorption. Journal of Colloid and Interface Science, 269(2), 310-314.

[32] Haldhar, R., & Prasad, D. (2020). Corrosion resistance and surface protective performance of waste material of Eucalyptus globulus for low carbon steel. Journal of Bio-and Tribo-Corrosion, 6(2), 48.

[33] Han, R., Zhang, J., Zou, W., Shi, J., & Liu, H. (2005). Equilibrium biosorption isotherm for lead ion on chaff. Journal of Hazardous materials, 125(1-3), 266-271.

[34] Hasan, S. K., & Sisodia, P. (2011). Paniala (Flacourtia Jangomas) Plant Extract as Eco-Friendly Inhibitor on the Corrosion of Mild Steel in Acidic Media. Rasayan Journal of Chemistry. 4(3), 548-553

[35] Hussin, M. H., Rahim, A. A., Mohamad Ibrahim, M. N., & Brosse, N. (2015). The Capability of Ultrafiltrated Alkaline and Organosolv Oil Palm (Elaeis guineensis) Fronds Lignin as Green Corrosion Inhibitor for Mild Steel in 0.5 M HCl Solution. Measurement, 78, 90-103. https://doi.org/10.1016/j.measurement.2015.10.007

[36] Ji, G., Dwivedi, P., Sundaram, S., Prakash, R. (2016). Aqueous Extract of Argemone Mexicana Roots for Effective Protection of Mild Steel in an HCl Environment. Research Chemical Intermediate, 42, 439–459. https://doi.org/10.1007/s11164-015-2029-y

[37] Kalam, S., Abu-Khamsin, S. A., Kamal, M. S., & Patil, S. (2021). Surfactant adsorption isotherms: A review. ACS omega, 6(48), 32342-32348.

[38] Kausalya, T., Hazlina, H. (2020). Review on Corrosion Inhibitors for Oil and Gas Corrosion Issues. Journal of Applied Science, 3389; doi:10.3390/app10103389. www.mdpi.com/journal/applsci

[39] Kesavan, D., Gopiraman, M., & Sulochana, N. (2012). Green inhibitors for corrosion of metals: a review. Chem. Sci. Rev. Lett, 1(1), 1-8.

[40] Krishnaveni, K., & Ravichandran, J. (2014). Effect of aqueous extract of leaves of Morinda

Tinctoria on Corrosion Inhibition of Aluminium Surface in HCl Medium. Transactions of Nonferrous Metals Society of China, 24(8), 2704-2712. https://doi.org/10.1016/S1003-6326(14)63401-4

[41] Manamela, K. M., Murulana, L. C., Kabanda, M. M., & Ebenso, E. E. (2014). Adsorptive and DFT Studies of Some Imidazolium Based Ionic Liquids as Corrosion Inhibitors for Zinc in Acidic Medium. International Journal of Electrochemical Science, 9(6), 3029-3046. https://doi.org/10.1016/S1452-3981(23)07989-0

[42] Milonjić, S. K. (2007). A consideration of the correct calculation of thermodynamic parameters of adsorption. Journal of the Serbian chemical society, 72(12), 1363-1367.

[43] Mohamad, N. A. N., Arham, N. A., Jai, J., & Hadi, A. (2014). Plant extract as reducing agent in synthesis of metallic nanoparticles: a review. Advanced Materials Research, 832, 350-355.

[44] Nandiyanto, A. B. D., Putri, S. R., Anggraeni, S., & Kurniwan, T. E. G. U. H. (2022). Isotherm adsorption OF 3000-µm natural zeolite. Journal of Engineering Science and Technology, 17(4), 2447-2460.

[45] Nasrollahzadeh, M., Sajadi, S. M., & Khalaj, M. (2014). Green synthesis of copper nanoparticles using aqueous extract of the leaves of Euphorbia esula L and their catalytic activity for ligand-free Ullmann-coupling reaction and reduction of 4-nitrophenol. RSC Advances, 4(88), 47313-47318.

[46] N'diaye, A. D., & Kankou, M. S. A. (2020). Modeling of adsorption isotherms of pharmaceutical products onto various adsorbents: A Short Review. J. Mater. Environ. Sci, 11(8), 1264-1276.

[47] Negm, N., Kandile, N., Aiad, I., & Mohammad, M. (2011). New Eco-friendly Cationic Surfactants: Synthesis, Characterization, and Applicability as Corrosion Inhibitors for Carbon Steel in 1 N HCl. Colloids and Surfaces A: Physicochemical and Engineering Aspects, 391(1-3), 224-233. https://doi.org/10.1016/j.colsurfa.2011.09.032

[48] Obot, I.B., & Obi-Egbedi, N.O. (2010). An interesting and efficient green corrosion inhibitor for aluminium from extracts of Chlomolaena odorata L. in acidic solution. Journal of Applied Electrochemistry. 40, 1977–1984. https://doi.org/10.1007/s10800-010-0175-x

[49] Oguzie, E. E. (2007). Corrosion inhibition of aluminium in acidic and alkaline media by Sansevieria trifasciata extract. Corrosion Science, 49(3), 1527-1539.

[50] Okafor, P. C., & Ebenso, E. E. (2007). Inhibitive Action of Carica Papaya Extracts on the Corrosion of Mild Steel in Acidic Media and their Adsorption Characteristics. Pigment Resin Technology. 36(3), 134–140. doi:10.1108/03699420710748992

[51] Okafor, P. C., Ikpi, M., Uwah, I., Ebenso, E., Ekpe, U., & Umoren S. (2008). Inhibitory Action of Phyllanthus Amarus Extracts on the Corrosion of Mild Steel in Acidic Media. Corrosion Science 50 (8), 2310–2317. doi:10.1016/j.corsci.2008.05.009

[52] Okewale, A. O., & Olaitan, A. (2017). The Use of Rubber Leaf Extract as a Corrosion Inhibitor for Mild Steel in Acidic Solution. International Journal of Materials and Chemistry, 7 (1), 5–13.

[53] Saadi, R., Saadi, Z., Fazaeli, R., & Fard, N. E. (2015). Monolayer and multilayer adsorption isotherm models for sorption from aqueous media. Korean Journal of Chemical Engineering, 32, 787-799.

[54] Shahbeig, H., Bagheri, N., Ghorbanian, S. A., Hallajisani, A., & Poorkarimi, S. (2013). A new adsorption isotherm model of aqueous solutions on granular activated carbon. World Journal of Modelling and Simulation, 9(4), 243-254.

[55] Shanavas, S., Kunju, A. S., Varghese, H. T., & Panicker, C. Y. (2011). Comparison of Langmuir and Harkins-Jura adsorption isotherms for the determination of surface area of solids. Oriental Journal of Chemistry, 27(1), 245.

[56] Sanatkumar, B., Nayak, J., & Nityananda Shetty, A. (2012). Influence of 2-(4-chlorophenyl)-2-oxoethyl benzoate on the Hydrogen Evolution and Corrosion Inhibition of 18 Ni 250 Grade Weld Aged Maraging Steel in 1.0 M Sulfuric Acid Medium. International Journal of Hydrogen Energy, 37(11), 9431-9442. https://doi.org/10.1016/j.ijhydene.2012.02.165

[57] Savran, A., Selçuk, N., Kubilay, Ş., & Kul, A. (2017). Adsorption isotherm models for dye removal by paliurus spinachristi mill. frutis and seeds in a single component system. IOSR J.

Environ. Sci. Toxicol. Food Technol, 11(04), 18-30.

[58] Saxena, A., Prasad, D., Haldhar, R., Singh, G., & Kumar, A. (2018). Use of Saraca ashoka extract as green corrosion inhibitor for mild steel in 0.5 M H2SO4. Journal of Molecular Liquids, 258, 89-97.

[59] Seo, J., Lee, S., Elam, M. L., Johnson, S. A., Kang, J., & Arjmandi, B. H. (2014). Study to find the best extraction solvent for use with guava leaves (Psidium guajava L.) for high antioxidant efficacy. Food science & nutrition, 2(2), 174-180.

[60] Shahbeig, H., Bagheri, N., Ghorbanian, S. A., Hallajisani, A., & Poorkarimi, S. (2013). A new adsorption isotherm model of aqueous solutions on granular activated carbon. World Journal of Modelling and Simulation, 9(4), 243-254.

[61] Sahmoune, M. N. (2019). Evaluation of thermodynamic parameters for adsorption of heavy metals by green adsorbents. Environmental Chemistry Letters, 17(2), 697-704.

[62] Sharghi, H., Khalifeh, R., & Doroodmand, M. M. (2009). Copper nanoparticles on charcoal for multicomponent catalytic synthesis of 1, 2, 3-Triazole derivatives from benzyl halides or alkyl halides, terminal alkynes and sodium azide in water as a “Green” solvent. Advanced Synthesis & Catalysis, 351(1-2), 207-218.

[63] Shivangi, G. (2022). Organic and Eco-friendly Corrosion Inhibitors for Sweet and Sour conditions (Investigation of corrosion inhibition mechanisms using experimental and molecular modeling). Technical University of Denmark.

[64] Singh, A., Kumar, A. S. H. I. S. H., & Pramanik, T. A. N. A. Y. (2013). A theoretical approach to the study of some plant extracts as green corrosion inhibitor for mild steel in HCl solution. Oriental Journal of Chemistry, 29(1), 277-283.

[65] Sultan, E. B., Areef, K., Abazeid, M., Khalil, E., Mahklouf, M., & Shushni, M. (2022). Cynodon dactylon L. extract as an eco-friendly corrosion inhibitor of mild steel in saline solution. Journal of Pharmacy & Bioresources, 19(2), 51-57.

[66] Sun, Z., Singh, A., Xu, X., Chen, S., Liu, W., & Lin, Y. (2017). Inhibition Effect of Pomelo Peel Extract for N80 Steel in 3.5% NaCl Saturated with CO2 Solution. Research on Chemical Intermediate, doi: 10.1007/s11164-017-3017-1.

[67] Tran, H. N., Lima, E. C., Juang, R. S., Bollinger, J. C., & Chao, H. P. (2021). Thermodynamic parameters of liquid–phase adsorption process calculated from different equilibrium constants related to adsorption isotherms: A comparison study. Journal of Environmental Chemical Engineering, 9(6), 106674.

[68] Vadi, M., Mansoorabad, A. O., Mohammadi, M., & Rostami, N. (2013). Investigation of Langmuir, Freundlich and Temkin adsorption isotherm of tramadol by multi-wall carbon nanotube. Asian Journal of Chemistry, 25(10), 5467.

[69] Varma, R. S. (2016). Greener and sustainable trends in synthesis of organics and nanomaterials.

[70] Varshney, V., Verma, A., Kumar, V., & Singh, T.P. (2023). A Review Paper on Green Corrosion and its Inhibitors. International Journal of Materials Science, 4(1): 27-31

[71] Velázquez-González, M. A., Gonzalez-Rodriguez, J. G., Valladares-Cisneros, M.G., & Hermoso-Diaz, I. A. (2014). Use of Rosmarinus Officinalis as Green Corrosion Inhibitor for Carbon Steel in Acid Medium. American Journal of - Analytical Chemistry. 5(2), 55-64.

[72] Vedantu, (01/05/2024). https://www.vedantu.com/chemistry/isotherm

[73] Vijayaraghavan, K. T. V. N., Padmesh, T. V. N., Palanivelu, K., & Velan, M. (2006). Biosorption of nickel (II) ions onto Sargassum wightii: application of two-parameter and three-parameter isotherm models. Journal of hazardous materials, 133(1-3), 304-308.

[74] Wang, Q., Tan, B., Bao, H., Xie, Y., Mou, Y., Li, P., Chen, D., Shi, Y., Li, X., & Yang, W. (2019). Evaluation of Ficus tikoua leaves extract as an eco-friendly corrosion inhibitor for carbon steel in HCl media. Bioelectrochemistry, 128, 49-55.

[75] Wei, H., Heidarshenas, B., Zhou, L., Hussain, G., Li, Q., & Ostrikov, K. K. (2020). Green Inhibitors for Steel Corrosion in Acidic Environment: State of Art. Materials Today Sustainability. 10, 100044. doi:10.1016/j.mtsust.2020.100044

[76] sZaabar, A., Aitout, R., Makhloufi, L., Belhamel, K., & Saidani, B. (2014). Inhibition of acid corrosion of mild steel by aqueous nettle extracts. Pigment & resin technology, 43(3), 127-138.